CATHODIC PROTECTION OF STEEL COMPONENTS OF ARMOURED AMPHIBIOUS VEHICLES IN MARINE ENVIRONMENT

A THESIS SUBMITTED TO
THE GRADUATE SCHOOL OF NATURAL AND APPLIED SCIENCES
OF
MIDDLE EAST TECHNICAL UNIVERSITY

BY

RAUF AKSU

IN PARTIAL FULFILLMENT OF THE REQUIREMENTS
FOR
THE DEGREE OF MASTER OF SCIENCE
IN
METALLURGICAL AND MATERIALS ENGINEERING

FEBRUARY 2017

Approval of the thesis:

CATHODIC PROTECTION OF STEEL COMPONENTS OF ARMOURED AMPHIBIOUS VEHICLES IN MARINE ENVIRONMENT

submitted by **RAUF AKSU** in partial fulfillment of the requirements for the degree of **Master of Science in Metallurgical and Materials Engineering Department, Middle East Technical University** by,

Prof. Dr. Gülbin Dural Ünver _____
Dean, Graduate School of **Natural and Applied Science**

Prof. Dr. Cemil Hakan Gür _____
Head of Department, **Metallurgical and Materials Engineering**

Prof. Dr. İshak Karakaya _____
Supervisor, **Metallurgical and Materials Eng. Dept., METU**

Assist. Prof. Dr. Metehan Erdoğan _____
Co-Supervisor, **Materials Engineering Dept., AYBU**

Examining Committee Members:

Prof. Dr. Kadri Aydınol _____
Metallurgical and Materials Engineering Dept., METU

Prof. Dr. İshak Karakaya _____
Metallurgical and Materials Engineering Dept., METU

Assist. Prof. Dr. Metehan Erdoğan _____
Materials Engineering Dept., AYBU

Assist. Prof. Dr. Erkan Konca _____
Metallurgical and Materials Engineering Dept., Atılım University

Assist. Prof. Dr. Batur Ercan _____
Metallurgical and Materials Engineering Dept., METU

Date: 03/02/2017

I hereby declare that all information in this document has been obtained and presented in accordance with academic rules and ethical conduct. I also declare that, as required by these rules and conduct, I have fully cited and referenced all material and results that are not original to this work.

Name, Last name: Rauf Aksu
Signature :

ABSTRACT

CATHODIC PROTECTION OF STEEL COMPONENTS OF ARMOURED AMPHIBIOUS VEHICLES IN MARINE ENVIRONMENT

Aksu, Rauf
M.S., Department of Metallurgical and Materials Engineering
Supervisor: Prof. Dr. İshak Karakaya
Co-supervisor: Assist. Prof. Dr. Metehan Erdoğan
February 2017, 77 pages

Selected steel grades used in manufacturing the hulls of armoured amphibious vehicles were subjected to accelerated corrosion tests in artificial seawater. The electrochemical data were obtained via potentiodynamic tests. Polarization characteristics of the steel samples were used to collect data for cathodic protection simulation with sacrificial anodes. The current requirement in cathodic protection systems was calculated to determine the quantity of the anodes. The resulting potential distributions on the uncoated steel surfaces in seawater were evaluated to optimize the protection. The locations and sizes of the anodes were modified to obtain protective potentials on the exposed bare surfaces of the steel components.

Keywords: corrosion, cathodic protection, sacrificial anode, computer modeling, polarization tests

ÖZ

ZIRHLI AMFİBİK ARAÇLARDA ÇELİK PARÇALARIN DENİZ SUYUNDA KATODİK KORUMA UYGULAMASI

Aksu, Rauf
Yüksek Lisans, Metalurji ve Malzeme Mühendisliği Bölümü
Tez Yöneticisi: Prof. Dr. İshak Karakaya
Ortak Tez Yöneticisi: Yrd. Doç. Dr. Metehan Erdoğan
Şubat 2017, 77 sayfa

Zırhlı amfibik araçların gövdesinde kullanılan çelik türlerinin deniz suyu ortamında hızlandırılmış korozyon testleri yapıldı. Elektrokimyasal veriler potansiyodinamik testsler ile elde edildi. Çelik numunelerin polarizasyon karakteristikleri kurban anotlar ile katodik koruma simülasyonuna veri elde etmek için incelendi. Kurban anot sayısını tayin etmek için akım gereksinimi hesaplandı. Korumayı optimize etmek için kaplamasız çelik yüzeylerde potansiyel dağılımları değerlendirildi. Deniz suyuna maruz kalan çıplak çelik yüzeylerde koruma potansiyellerine ulaşmak için anotların konumları ve boyutları ayarlandı.

Anahtar Kelimeler: korozyon, katodik koruma, kurban anot, bilgisayar modellemesi, polarizasyon testleri



To my family

ACKNOWLEDGEMENTS

I would like to express my deepest gratitude cordially to my supervisor Prof. Dr. İshak Karakaya for his patience, motivation, guidance, advice, criticism, support and insight not only throughout this thesis but in many other studies.

I also wish to express my gratitude to Assist. Prof. Dr. Metehan Erdoğan for his guidance, advice, criticism, support and comments during this study.

I am sincerely grateful to Prof. Dr. Kadri Aydınol, Assist. Prof. Dr. Erkan Konca, and Assist. Prof. Dr. Batur Ercan for their suggestions, comments and support.

I would also like to thank the members of Thermochemical and Electrochemical Materials Processing Laboratory, especially Mustafa Serdal Aras and Furkan Özdemir for their support and assistance throughout this thesis.

I must express my very profound gratitude to Zeynep Elif Can Çayan for providing me with unfailing support and continuous encouragement throughout my years of study and through the process of researching and writing this thesis. This accomplishment would not have been possible without her.

Finally, I would like to acknowledge the technical and the financial support of FNSS Defence Systems and the financial support of Undersecretariat for Defence Industries of Republic of Turkey. The contents, ideas and opinions presented in this study do not necessarily reflect those of FNSS Defence Systems and Undersecretariat for Defence Industry.

TABLE OF CONTENTS

ABSTRACT v
ÖZ vi
ACKNOWLEDGEMENTS viii
LIST OF TABLES xi
LIST OF FIGURES xii
CHAPTERS
1. INTRODUCTION 1
1.1 Problem Statement 3
2. LITERATURE REVIEW 5
2.1 Introduction 5
2.2 Corrosion Thermodynamics 6
2.3 Electrode Kinetics 9
2.4 Corrosion of Steels in Seawater 14
2.5 Corrosion Testing 18
2.6 Corrosion Prevention 20
2.7 Numerical Modeling 28
3. EXPERIMENTAL STUDY 31
3.1 Materials 31
3.2 Electrolyte 32
3.3 Reference Electrode 33
3.4 Experimental Setup 33
4. RESULTS AND DISCUSSION 35
4.1 Electrochemical Tests 35
4.2 Numerical Modeling 42

5. CONCLUSIONS 65
REFERENCES 67
APPENDIX I 73
APPENDIX II 75
APPENDIX III 77

LIST OF TABLES

TABLES

Table 1 Recommended current density requirement for seawater exposed uncoated metal surfaces as a function of depth at subtropical environment (12-20 ^{o}C) [30].... 25
Table 2 Characteristics of available sacrificial anodes [36]..... 26
Table 3 Anode resistance formulae for cathodic protection design [30] 27
Table 4 Chemical compositions of selected steels. 31
Table 5 Artificial seawater constituents and concentrations. 32
Table 6 The overall mean results of electrochemical polarization tests in artificial seawater at 20^{o}C 35
Table 7 The limiting current density values derived from the Tafel plots 40
Table 8 Resultant corrosion rates according the cathodic polarization..... 46
Table 9 Anode parameters and seawater resistivity in CP system 47
Table 10 Overall parameters of corrosion kinetics used in modeling..... 51

LIST OF FIGURES

FIGURES

Figure 1 German M3 Amphibious Bridging and Ferrying System [4] 2
Figure 2 Corroded surfaces on the steel components of an amphibious vehicle 3
Figure 3 The average ion concentrations of seawater and river water. Reproduced from [8] 5
Figure 4 Typical electrochemical cell in equilibrium with their ions separated by a porous membrane 7
Figure 5 A schematic of the transport of an electron in reduction and oxidation reactions 10
Figure 6 A schematic polarization curve for metal M in a solution containing H^+ ... 11
Figure 7 A schematic of a mixed electrode kinetics behavior of metal M in acid solution 12
Figure 8 A schematic effect of concentration polarization on Tafel plot 14
Figure 9 The potential-pH diagram of iron in water for 10^{-6} M activities of all metal ions. Reproduced from [23] 15
Figure 10 A schematic of the Pourbaix diagram indicating corrosion regions for iron 16
Figure 11 The combined effects of cathodic polarizations 18
Figure 12 A schematic illustration of an experimental arrangement for a laboratory electrochemical polarization tests 19
Figure 13 A schematic plot illustrating the Tafel extrapolation method 20
Figure 14 Cathodic protection by applied current density 22
Figure 15 Galvanic series of different materials for seawater (active behavior of active-passive alloys is indicated by dark boxes) reproduced from [34] 24
Figure 16 A typical construction of a calomel electrode 33
Figure 17 A schematic of the corrosion cell setup together with the potentiostat 34

Figure 18 Potentiodynamic polarization curve for S355 JR in artificial seawater at 20 ºC 36
Figure 19 Potentiodynamic polarization curve for AISI 1010 in artificial seawater at 20 ºC 36
Figure 20 Potentiodynamic polarization curve for AISI 4140 in artificial seawater at 20 ºC 37
Figure 21 The Tafel extrapolation method applied manually to AISI 4140 38
Figure 22 The cathodic branch and the limiting current plateau of Tafel Plot of AISI 4140 40
Figure 23 Determination of the limiting current density value by the derivative method for AISI 4140. The specific region on the cathodic branch of the polarization curve (a) and the first derivate di/dE of the polarization curve (b) are used. 41
Figure 24 The quarter part of the vehicle geometry, (a) isometric transparent view with dimensions in 10^3 mm, (b) side view, (c) bottom view 43
Figure 25 Steel components of the selected quarter of the hull structure 44
Figure 26 Polarization of AISI 4140 to the different protection potentials 45
Figure 27 Boundary conditions for cathodic protection model 51
Figure 28 Meshed model geometry 52
Figure 29 Statistics on mesh quality 53
Figure 30 Element size parameters 54
Figure 31 Convergence plot of nonlinear solver 55
Figure 32 Highlighted anodes in the vehicle hull 56
Figure 33 Relative anode positions in millimeters in the vehicle hull on xy plane 56
Figure 34 The resulting potential distribution on the steel surfaces with 8 anodes 57
Figure 35 Additional pencil anodes placed near the wheel hub 58
Figure 36 Comparison of the effectiveness of different situations on the wheel hub: existing (left), designed (center) and modified (right) systems 59
Figure 37 The locations of uncoated areas in the hull structure 60
Figure 38 The resulting potential distribution on the uncoated steel surfaces 61
Figure 39 Pencil anodes' loactions for reduced steel area 62
Figure 40 The reduced amount of anodes for paint deficient areas 63

CHAPTER 1

INTRODUCTION

An amphibious vehicle is a wheeled or tracked vehicle which is capable of operating both in land and water [1]. Amphibious armored military vehicles are designed to deliver infantrymen with their equipment in amphibious operations, which are launched within littorals by armed forces to conduct landing operations on a hostile shore. There is a wide variety of amphibious operations:

- Amphibious raid
- Amphibious demonstration
- Amphibious assault
- Amphibious withdrawal
- Amphibious force support to crisis response and other operations

Conducting these operations requires amphibious force which consists of an amphibious task and a landing force along with other trained, organized and equipped forces [2].

There are some difficulties that restrict movements and maneuvers of vehicles and staff. Linear obstacles are one of the challenging obstacles since transporting combat power across a linear obstacle, called gap crossing is critical to enable armed forces to manage their operations. Types of gaps are ravine, mountain pass, river or other terrain conditions that present an obstacle which is needed to be crossed over. River crossing is one of the most challenging types of gap crossing. To overcome various obstacles, there are several crossing solutions available including fording, swimming and amphibious vehicles [3].

However, most of the military vehicles are not capable of fording or swimming in deep water. There is a need for bridges or ferries to transport non-amphibious vehicles and equipment to the far side of a water obstacle.

Specialized engineering type of military amphibious vehicles can enable transportation of land vehicles such as tanks, armored personnel carriers and assault vehicles through the wet gaps such as rivers and lakes. Advanced military units and armed forces keep amphibious bridging and ferrying systems in their inventory. For example, German designed M3 amphibious rig, shown in Figure 1, is currently in use in the German and British armed forces.



Figure 1 German M3 Amphibious Bridging and Ferrying System [4]

Military vehicles are operated at harsh and tough conditions. There may be some damages on the vehicle body due to high shock and vibration over rough terrain, explosive blast, ballistic impact etc. [5].

Protective coating on the surface of metal structures may fail by means of chalking, blistering, peeling and spalling [6]. The bare metal surfaces get corroded unless there is an external protection system.

1.1 Problem Statement

Corrosion has always been a pertinacious problem to engineers in many fields of industry. According to the Department of Defence (DoD), there are several factors affecting physical assets including buildings, military equipment and assault vehicles due to degradation of metals. Safety issues, such as structural instabilities in facilities and weapon system mishaps, have been experienced due to corrosion related failures. Sometimes military equipment and infrastructures are rejected by committee because of corrosion deficiencies. The overall cost of corrosion and associated disbursement of damage repair or replacement parts can be minimized by preventing corrosion [7].

In some cases, the design of a vehicle or a system is not appropriate for varying service environment. The materials selection of the vehicle could be made without considering any corrosive medium. Thus, supplementary protection systems should be applied to the exposed surfaces of bare steel components in aggressive surroundings such as seawater. As seen in Figure 2, the supporting rod of a vehicle was corroded when a cathodic protection system was not present on the hull of the vehicle. In fact, this vehicle was designed to use in fresh water. However, it is expected for a military amphibious vehicle to adapt and operate without obtrusive incidents in various conditions including seawater for many years.

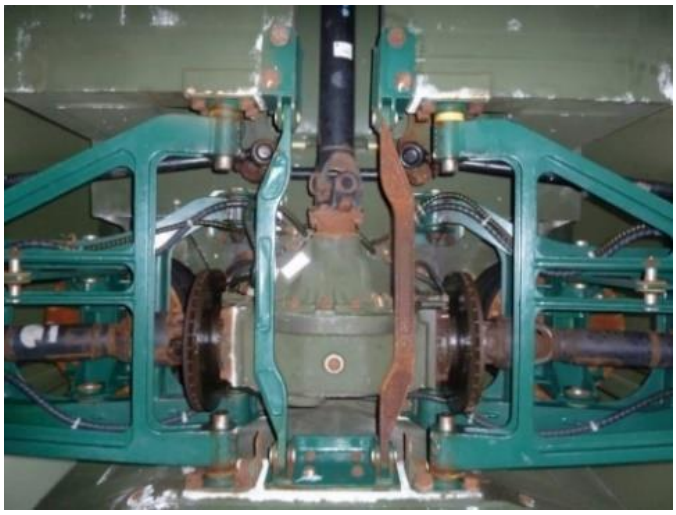


Figure 2 Corroded surfaces on the steel components of an amphibious vehicle

In this study, the corrosion behavior of selected steel components of an armored amphibious vehicle was investigated. The effectiveness of a cathodic protection system installed on the vehicle hull was studied through numerical modeling by creating several cases having various total paint deficient areas in marine environment. Finally, smaller sacrificial anodes were attached to the necessary places to ensure the homogeneity of protection potential near the problematic regions.

CHAPTER 2

LITERATURE REVIEW

2.1 Introduction

Corrosion is a form of metal degradation process due to chemical or electrochemical interactions with the surrounding environment. Uncoated surfaces of hull structures of amphibious vehicles are exposed to corrosion during operations. Corrosion tends to accelerate in brackish or seawater, which contains more dissolved salts than in fresh or river water. Figure 3 shows the average concentrations of dissolved constituents in seawater and river water. The concentrations of dissolved salts in an average seawater (34400 mg/l) are about 300 times higher than those in an average river water (118.2 mg/l) [8].

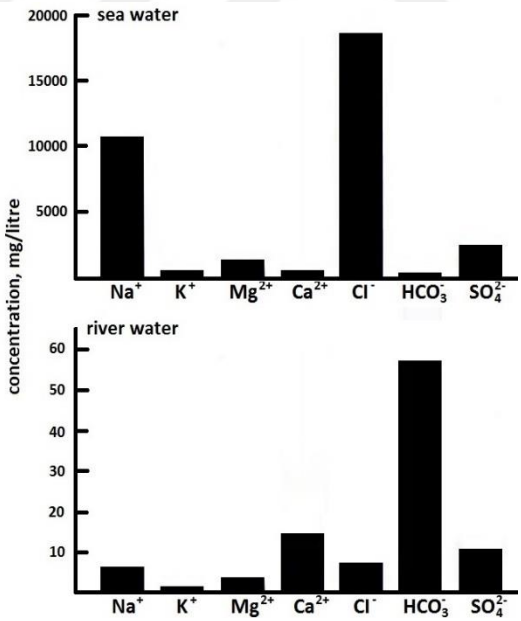


Figure 3 The average ion concentrations of seawater and river water. Reproduced from [8]

This thesis addresses the corrosion problems associated with changing operational environment of military amphibious vehicles from fresh water to marine. The corrosion behavior and cathodic protection of carbon and low alloy steels when submerged in seawater, which is a more corrosive environment than the average river water, were investigated within the scope of this study. In this chapter, basic principles of corrosion including thermodynamics relations and electrode kinetics were mentioned. In addition, corrosion prevention methods were briefly introduced and a specific focus was given to cathodic protection with sacrificial anodes to prevent corrosion of steels in seawater.

2.2 Corrosion Thermodynamics

Thermodynamic principles of aqueous corrosion are reviewed to understand electrochemical relations of electrodes in marine environment. First of all, the concept of the change in Gibbs Energy depends on the possibility of a reaction to occur. Spontaneous transition of a system from one state to another is caused by the negative change in free energy. Positive change, on the other hand, indicates that some amount of energy need to be added to the system for reaction to occur [9].

The sign of the change in Gibbs Energy (ΔG) states the tendency of an electrochemical reaction to go either in forward or backward direction. It is also possible to express the corrosion tendency of a metal in terms of the electromotive force (emf) [10]. The relation between the change in Gibbs Energy and the emf of an electrochemical reaction, E, can be calculated by the following equations

$$\Delta G = \text{charge passed} \times \text{cell potential}$$

$$\Delta G = -nFE \quad (1)$$

where n is the number of electrons participated in the reaction and F is the Faraday constant (96485 coulombs/mole-electrons).

Half-Cell Potential and emf of a Cell

The change in Gibbs Energy is directly related to the potential difference between two electrodes, which is defined as the emf of a cell. The direction of an overall electrochemical reaction in a complete cell is determined by the sign of the emf, which is equal to the summation of half-cell voltages. As can be seen in equation 1, a positive emf indicates a negative ΔG and therefore, a spontaneous reaction. To illustrate, a half-cell having the most negative emf tends to be oxidized and the most positive half-cell tends to be reduced [9]. An electrochemical cell can be divided into two distinct oxidation and reduction half reactions as illustrated in Figure 4. The two representative individual half-cell reactions are written below.

$$aRed_1 \rightarrow bOxi_1 + ne^- \quad (2)$$

$$cOxi_2 + ne^- \rightarrow dRed_2 \quad (3)$$

In the first reaction, species of Red_1 is oxidized to Oxi_1 by giving n electrons. The latter reaction dictates that species of Oxi_2 is reduced to Red_2 by taking n electrons [11].

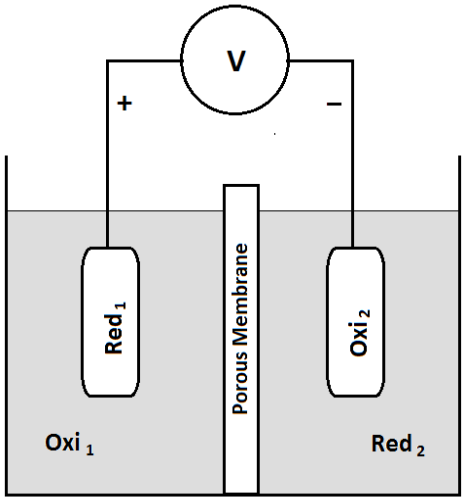


Figure 4 Typical electrochemical cell in equilibrium with their ions separated by a porous membrane

The representation of the overall cell reaction, consisting of two independent half reactions is

$$aRed_1 + cOxi_2 \rightarrow bOxi_1 + dRed_2 \tag{4}$$

In this reaction "a" moles of Red_1 and "c" moles of Oxi_2 are reactants; "b" moles of Oxi_1 and "d" moles of Red_2 are products. The change of Gibbs free energy for the reaction is calculated by subtracting the molar Gibbs Energy of products from the reactants.

$$\Delta G = (bG_{Oxi1} + dG_{Red2}) - (aG_{Red1} + cG_{Oxi2}) \tag{5}$$

If all substances are in their standard states, the standard molar free energy is denoted by G^o.

$$\Delta G^o = (bG^o{}_{Oxi1} + dG^o{}_{Red2}) - (aG^o{}_{Red1} + cG^o{}_{Oxi2}) \tag{6}$$

Subtracting equation 5 from 6, to find the difference between the Gibbs Energy change in any state and the standard state, gives

$$\Delta G - \Delta G^o = RTln\frac{a_{Oxi1}^b \cdot a_{Red2}^d}{a_{Red1}^a \cdot a_{Oxi2}^c} \tag{7}$$

The symbols a_i, R and T represent the activities of the substances, the gas constant and temperature in Kelvin, respectively. When all substances are in their standard states, the equation (1) can be rewritten as

$$\Delta G^o = -nFE^o \tag{8}$$

Substituting the Gibbs Energy terms in the equation (7) by the emf, gives the following expression.

$$E = E^o - \frac{RT}{nF}ln\frac{a_{Oxi1}^b \cdot a_{Red2}^d}{a_{Red1}^a \cdot a_{Oxi2}^c} \tag{9}$$

Therefore, the emf of a cell can be expressed in terms of concentration of reactants and products of the overall reaction because activities are composition dependent quantities. Equation (9) is called as the Nernst equation.

The emf of a cell can be measured by a high impedance voltmeter. It is critical to avoid polarization due to current flow because measurements would be more accurate when the cell is reversible. A cell can be reversible when each half-cell is at local equilibrium [10].

The emf of a reaction can be determined by measuring the voltage in a cell between oxidizing and reducing substances, electrodes. In addition, potential of each electrode relative to an electrode of constant potential, which is called as the reference electrode, can be measured to yield half-cell potentials of electrode reactions [11].

Thermodynamics, herewith, can signify the spontaneity of the electrochemical reaction. However, negative change in Gibbs free energy or positive emf of the corrosion reaction is not always being indicative of metal oxidation. The forward direction may be favored but the reaction rates can be extremely slow suggesting that corrosion will not occur.

2.3 Electrode Kinetics

The rate of a corrosion reaction is characterized by electrode kinetics. Corrosion occurs at the interface between a metal and an electrolyte. Metal dissolution or metal oxide formation and a reduction reaction, in a corrosion cell, take place simultaneously at the surfaces of an active metal (anode) and relatively noble material (cathode), respectively. Anodic and cathodic reactions may occur on the same surface as well, due to non-homogeneity of corroding metal [12]. As seen in Figure 5, electrons are released from the dissolving metal and transferred to the lowest unoccupied energy level of a reactant species through the solution in a reduction reaction. Whereas, electrons are transferred from the highest energy level of the reactant to the electrode through the solution in an oxidation reaction [13].

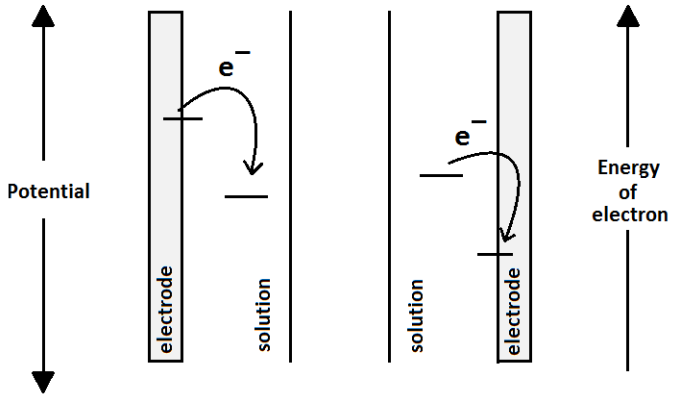


Figure 5 A schematic of the transport of an electron in reduction and oxidation reactions

The potentials at the two electrodes are not at equilibrium because of the electron interactions. Polarization is defined as the deviation from equilibrium potential due to a net current in a short circuited electrochemical cell. The difference between the actual potential (V) and the equilibrium potential ($\phi_{equilibrium}$) of an electrode is expressed as over-potential (η) [9].

$$\eta = V - \phi_{equilibrium} \tag{10}$$

Over-potential is the driving force for corrosion reactions. The rate of an oxidation or a reduction reaction occurring at the electrode surface is proportional to the current. The net rate is equal to the difference between anodic reaction rate and cathodic reaction rate and proportional to the current density.

$$rate = \frac{i_{net}}{nF} \tag{11}$$

The dependence of the rate (or current density) on over-potential can be calculated by the Butler-Volmer equation.

$$i = i_0 \left[exp\left(\frac{\alpha_a F}{RT}\eta\right) - exp\left(-\frac{\alpha_c F}{RT}\eta\right)\right] \tag{12}$$

where i is the current density, i_0 is the exchange current density, α_a and α_c are the anodic and cathodic transfer coefficients, F is the Faraday constant, and T is the temperature in Kelvin. The derivation of the Butler-Volmer equation will be mentioned further in following chapters.

The polarization behavior of a metal M in an acidic solution is shown in Figure 6. For small values of polarization, it can be presumed that the current density (log*i*) varies linearly with over-potential, whereas it varies exponentially for large values of over-potential [14].

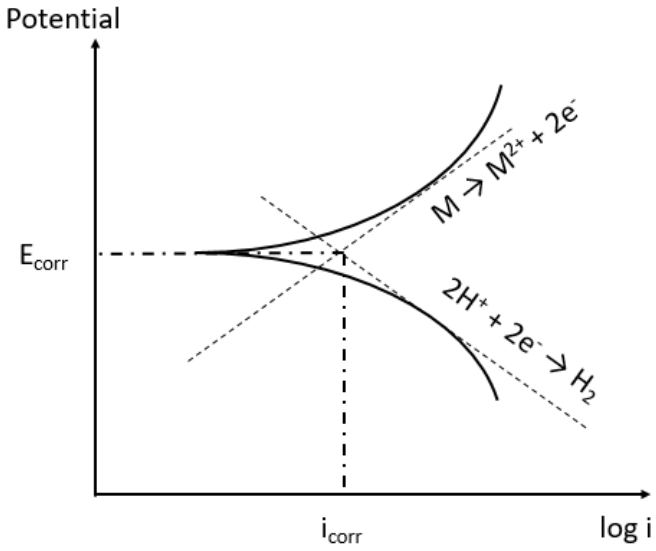


Figure 6 A schematic polarization curve for metal M in a solution containing H^+

The logarithmic relation between current density and over-potential was discovered by Tafel in 1905 [15]. A plot of potential versus logarithm of current density, given in Figure 6, is generated by using the Butler-Volmer equation and named as Tafel plot. The interpretation of the "Tafel slopes" for both anodic and cathodic reactions reveals a vast amount of information on corrosion kinetics [16].

Mixed Potential Theory

The mixed potential theory can be described with mixed electrodes on which two or more oxidation and reduction reactions are occurring. It could be exemplified as immersing an active metal into an acid solution. The theory consists of two basic hypotheses [9]. The first one states that two or more electrochemical reactions may occur simultaneously on surface of a metal or dissimilar metals in a solution. The overall potential which is resulted from corrosion process is defined as mixed or corrosion potential. The second hypothesis declares that the net current or current density becomes zero when the sum of total anodic currents and the total cathodic currents are equal at this potential. The conservation of charge is balanced by the net reaction rates of anode and cathode [13]. In Figure 7, electrochemical reactions of corroding metals M_1 and M_2 when coupled in same solution are represented in a graphical form called Evans diagram.

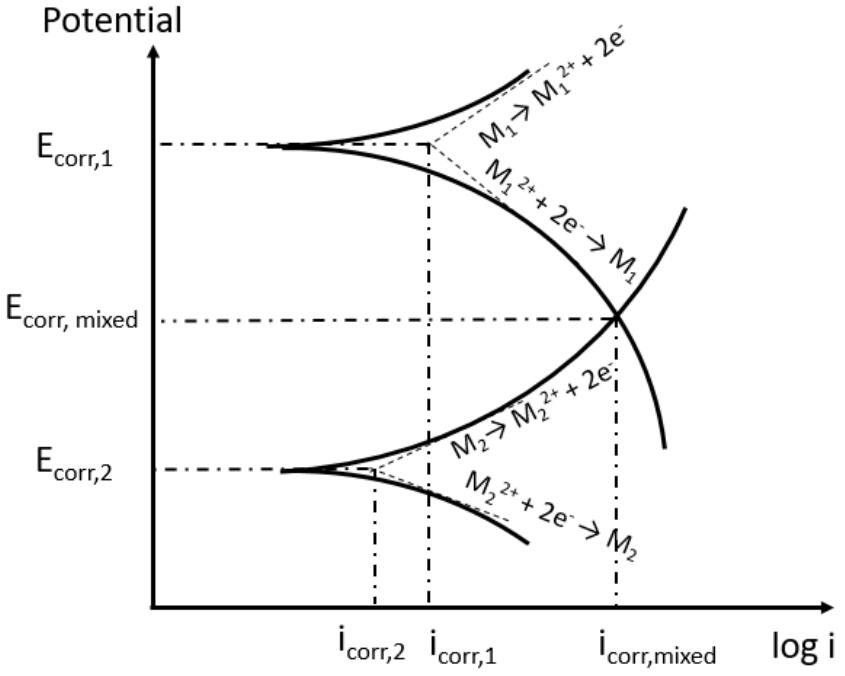


Figure 7 A schematic of a mixed electrode kinetics behavior of metal M in acid solution

When the metal is in equilibrium with its ions, a reversible potential (E_{corr}) and corresponding exchange current density (i_{corr}) result from the reactions below.

$$M \rightarrow M^{2+} + 2e^{-} \qquad \text{and} \qquad M^{2+} + 2e^{-} \rightarrow M \tag{13}$$

Graphical examination of the electrode kinetic behavior of the metals in solution reveals that the total rates of oxidation and reduction reactions are equal at a single value which indicates the mixed or corrosion potential ($E_{corr,mixed}$) and the current density ($i_{corr,mixed}$) [9]. The rate of corrosion reactions can be calculated from the slope of the total current-potential density diagram at the mixed potential under certain assumptions. Wagner and Traud [17] developed a graphical method to determine the mixed potentials. The method suggests that corrosion potential and corrosion current can be determined approximately as the intercept by extrapolating both anodic and cathodic partial polarization curves [18].

Concentration Polarization

The concentration of a species in electrolyte can control the rate of the corrosion in some cases. The cathodic reactions in an electrochemical cell cause polarization due to the ionic mass transfer from the bulk solution to the metal interface [19]. The corrosion kinetics changes when the surface concentration of a reactant species is not the same as the bulk solution. As illustrated in Figure 8, the cathodic branch of the Tafel plot is altered for a corroding metal in an electrolyte where the rate of reaction is controlled by diffusion of oxygen to the surface.

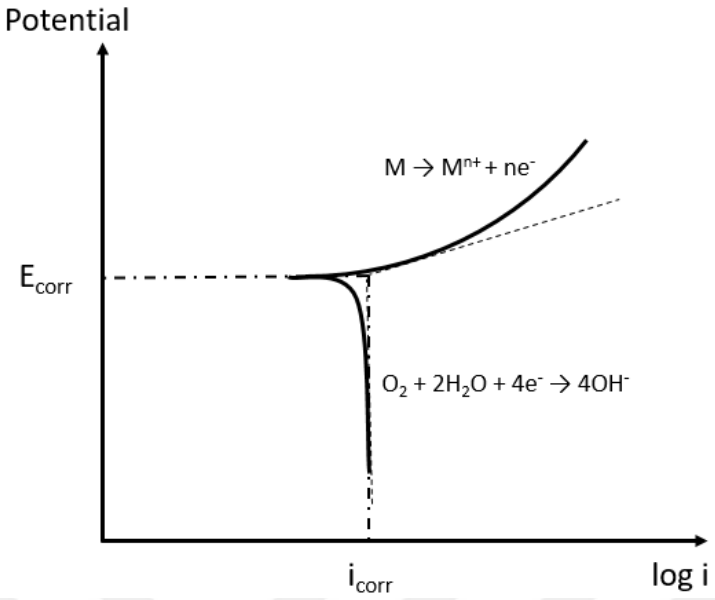


Figure 8 A schematic effect of concentration polarization on Tafel plot

Oxygen reduction as a cathodic reaction is very common in corroding systems. As molecular oxygen is reduced at the metal surface, the concentration of the dissolved oxygen in the electrolyte near the surface is decreased. Therefore, the transport of the dissolved oxygen from the bulk solution to the adjacent boundary is necessary for the reaction to continue [20].

2.4 Corrosion of Steels in Seawater

Steel structures in marine environment may suffer from corrosion on five different zones; which are atmospheric, splash, tidal, submerged and seabed-embedded zones. The rate of steel corrosion is affected by several seawater properties including salinity, temperature, pH, dissolved oxygen concentration, biological organisms etc. These variables of seawater can depend on each other, for example; oxygen concentration in seawater is greatly affected by temperature [21].

Degradation of a metal when exposed to an aqueous environment depends on the stability of the metal which may vary with the pH of the environment. The effect of aqueous electrolytes on corrosion behavior of a metal was introduced by Pourbaix [22]. A predominance or Pourbaix diagram represents the relation between potential

of the metal (E) and pH of the solution to show stable species in aqueous solutions. The use of E-pH diagrams allows to predict whether corrosion can occur or not; to estimate the form of corrosion products and predict if the environmental changes prevent or reduce corrosion [23].

Pourbaix Diagram of Iron

The Pourbaix diagram of iron in water at 25°C is shown in Figure 9. Water is thermodynamically stable between the dashed lines which are superimposed on all potential-pH diagrams.

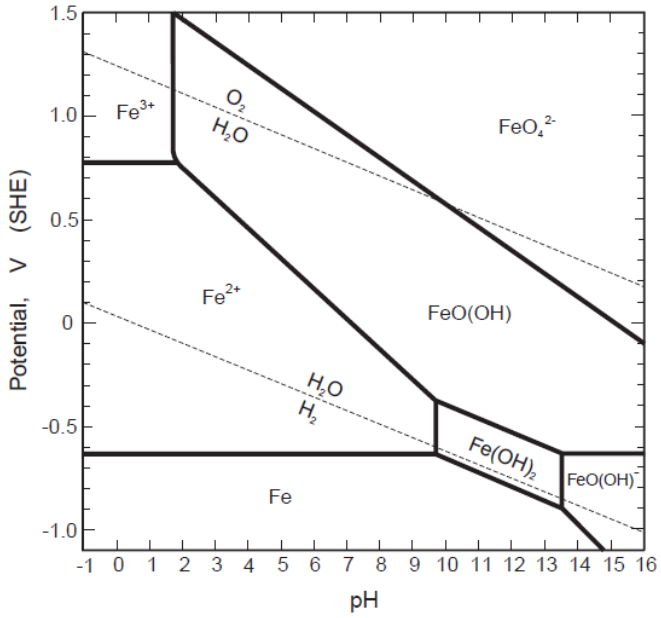


Figure 9 The potential-pH diagram of iron in water for 10^{-6} M activities of all metal ions. Reproduced from [23]

Horizontal lines in the Pourbaix diagram are independent of pH. Hydrogen ions are not involved in the equilibrium. The line between Fe^{2+} and Fe^{3+} is constructed with the Nernst equation by taking activities of Fe^{2+} and Fe^{3+} as 10^{-6} M.

$$Fe^{3+} + e^{-} \leftrightarrow Fe^{2+} \tag{14}$$

$$E = E^{o} - \frac{RT}{nF} ln \frac{[Fe^{2+}]}{[Fe^{3+}]} \tag{15}$$

Vertical lines do not involve oxidation and reduction reactions. The line between Fe^{2+} and $Fe(OH)_2$ represents the reaction below in the diagram.

$$Fe^{2+} + 2H_2O \leftrightarrow Fe(OH)_2 + 2H^+ \quad (16)$$

Sloping lines involve both electrons and hydrogen ions. For example, the line between Fe^{2+} and $FeO(OH)^-$ shows the equilibrium reaction below [24].

$$FeO(OH) + 3H^+ + e^- \leftrightarrow Fe^{2+} + 2H_2O \quad (17)$$

Corrosion of iron is possible in the regions where the soluble ions (Fe^{3+}, Fe^{2+} and $FeO(OH)^-$) are stable as shown in Figure 10.

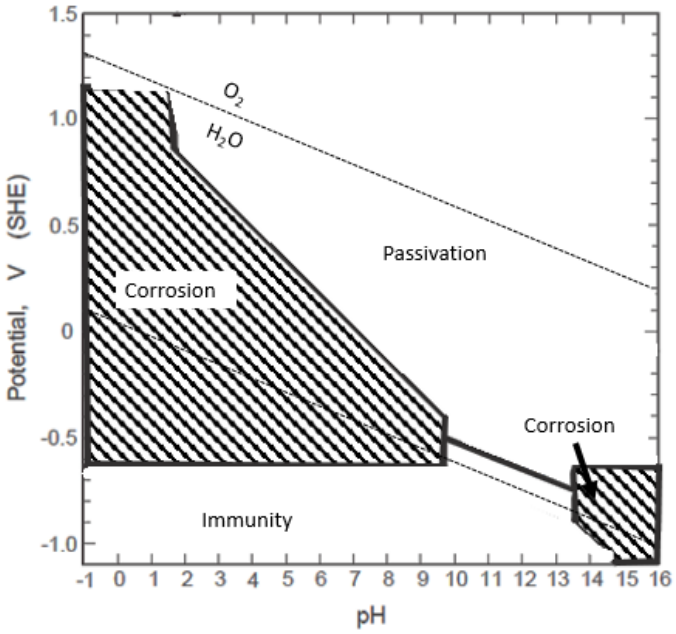


Figure 10 A schematic of the Pourbaix diagram indicating corrosion regions for iron

The stability region of iron oxide at elevated pH shows that iron is more resistant to alkaline environment. In nearly neutral pH with dissolved oxygen, the potential is shifted into passivation region where a protective oxide film is formed. Yet, below the neutral potential, this film is not stable [25].

Possible Reactions on the Steel Surfaces

Iron dissolution on uncoated boundaries can occur as the anodic process in many forms including the reaction given below.

$$Fe \rightarrow Fe^{2+} + 2e^{-} \tag{18}$$

The ferrous hydroxide precipitates are formed from ferrous ions and water molecules or hydroxyl ions:

$$Fe^{2+} + 2H_2O \rightarrow Fe(OH)_2 + 2H^{+} \tag{19}$$

or

$$Fe^{2+} + 2OH^{-} \rightarrow Fe(OH)_2 \tag{20}$$

The electrons released by the dissolution of iron must be consumed by cathodic reactions in which dissolved oxygen is oxidizing agent:

$$O_2 + 4e^{-} + 2H_2O \rightarrow 4OH^{-} \tag{21}$$

or

$$O_2 + 4e^{-} + 4H^{+} \rightarrow 2H_2O \tag{22}$$

When the reactions occur on the same electrode surface, the overall corrosion equation becomes

$$2Fe + O_2 + 2H_2O \rightarrow 2Fe(OH)_2 \tag{23}$$

It is also possible that hydrogen ions can involve in corrosion process as an oxidizing agent in cathodic reactions:

$$2H^{+} + 2e^{-} \rightarrow 2H_2 \tag{24}$$

or

$$2H_2O + 2e^{-} \rightarrow H_2 + 2OH^{-} \tag{25}$$

The corrosion reaction can be rewritten as

$$Fe + 2H^+ \rightarrow Fe^{2+} + H_2 \quad (26)$$

or

$$Fe + 2H_2O \rightarrow 2Fe(OH)_2 + H_2 \quad (27)$$

Both oxygen reduction and hydrogen evolution reactions can occur on the metal surface simultaneously. The curve of the cathodic branch of a mixed electrode is then shaped by these equations as shown in Figure 11.

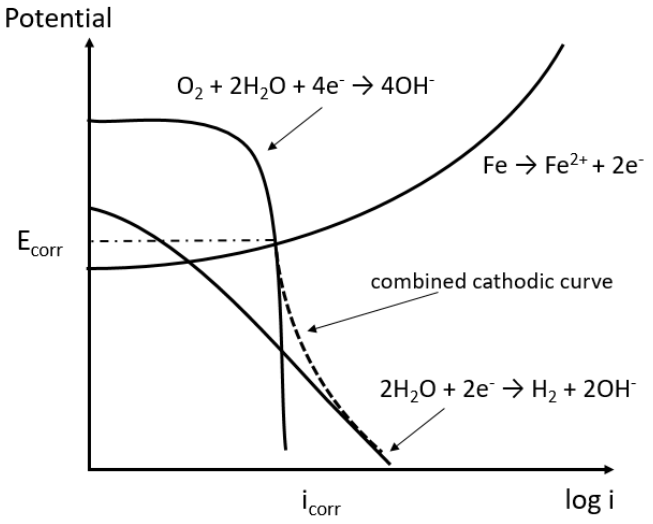


Figure 11 The combined effects of cathodic polarizations

The form of metal ions in dissolution reaction depends on many properties of seawater including the pH and dissolved oxygen concentration. Since properties of seawater vary by region, predicting the actual corrosion reactions might be difficult.

2.5 Corrosion Testing

The importance of corrosion testing in predicting possible failures or estimating service life time has been well understood in many industries. Corrosion tests should be reproducible and reliable. It is essential for the test to represent the actual conditions as closely as possible. Corrosion tests can be divided into four main categories: laboratory, pilot-plant, field and plant tests. In this study, only laboratory

testing is implemented to imitate the actual conditions. Laboratory tests are conducted on small specimens, so-called coupons, in small volumes of electrolyte solutions. Corrosion tests in laboratory are predominantly comprised of electrochemical test methods. Nevertheless, techniques such as immersion test or salt spray test reveal valuable information on corrosion characteristics [9,24].

Electrochemical tests can be categorized regarding the application of external current or potential perturbation. Corrosion or open circuit potential can be measured without external signal whereas polarization resistance or electrochemical impedance spectroscopy requires small signal polarization. In case of potentiostatic and potentiodynamic polarization measurements, applied signal should be larger [26].

Most of the laboratory electrochemical tests are performed on metal sample in electrochemical cells by a potentiostat. The other main equipment, which need to be used in a complete test set-up as given in Figure 12, are counter electrode, reference electrode, and computer with a recorder and plotter featured software.

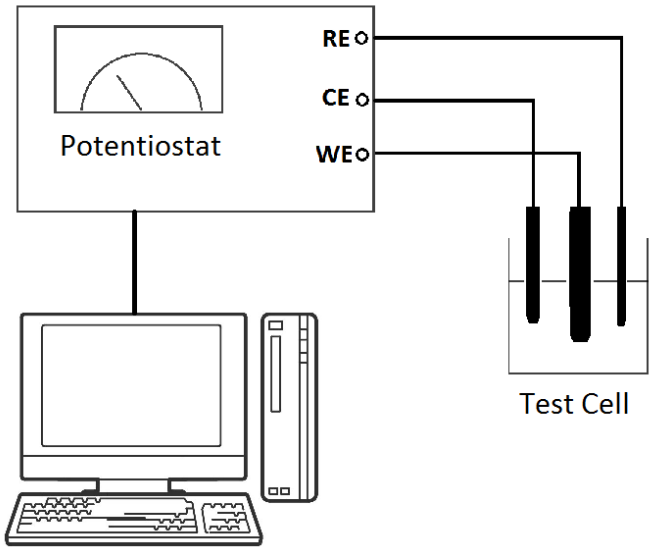


Figure 12 A schematic illustration of an experimental arrangement for a laboratory electrochemical polarization tests

Large-signal polarization tests were preferred for laboratory electrochemical measurements in this study. The potential was varied over a specified range at a

constant rate or a series of applied potential steps in this type of accelerated corrosion test. A polarization curve, obtained by the potentiodynamic technique, consists of anodic and cathodic branches. The result of the tests is interpreted to obtain corrosion kinetic parameters. The corrosion current density is determined by extrapolation of anodic and cathodic slopes of the curves near corrosion or open-circuit potential. In this technique, namely Tafel extrapolation method illustrated in Figure 13, it is possible to extract many valuable electrochemical data such as anodic and cathodic Tafel slopes, corrosion potential and corrosion current from a simple polarization curve [14,26].

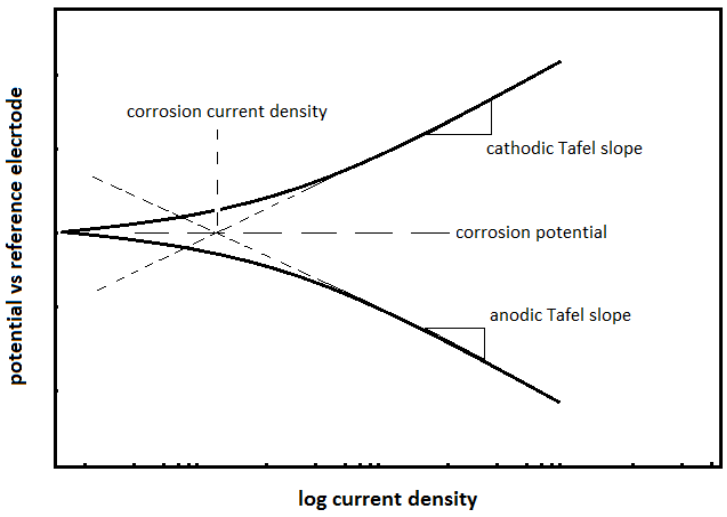


Figure 13 A schematic plot illustrating the Tafel extrapolation method

2.6 Corrosion Prevention

Corrosion causes troublesome problems on metal structures in marine environment. Oxidation of metals in seawater can be controlled with several precautions. The five main methods to prevent corrosion are [27]:

- Isolating metal from seawater by application of coating
- Regulate potential of metal by electrochemical methods
- Alteration of environment with corrosion inhibitors
- Choice of appropriate materials for marine conditions
- Proper assembly or system design

Generally, the most suitable corrosion prevention methods are chosen based on economic considerations. Yet, appearance, environment and safety are also remarkable factors. Applicability of prevention method is also a very important factor. Corrosion problem may come out unexpectedly on poorly designed structures during service. Change of environment by adding inhibitors is impracticable in marine conditions. Electrochemical protection methods can be applied when corrosion problem has arisen in order to compensate isolation defects and material interactions or change of medium such as fresh water to saline environment.

Cathodic Protection

Cathodic protection (CP) is defined by NACE RP0176 as "a technique to reduce corrosion of a metal surface by making that surface the cathode of an electrochemical cell" [28]. It is a widely used practical electrochemical method for iron and steels because of its easy application and low maintenance requirement.

The basis for cathodic protection is regulating the potential of the protected metal in order to polarize it cathodically by an external current source. When the uncoated metal in corrosive medium is polarized beyond the protection potential, the corrosion rate becomes almost zero on the metal surfaces. As illustrated in Figure 14, if the corrosion potential of the metal is decreased from E_{corr} to E_{CP} by the applied current, the corrosion current density decreases from i_{corr} to i_{CP}. An increase in the applied current results in smaller corrosion current densities, hence the corrosion is significantly reduced or eliminated [10].

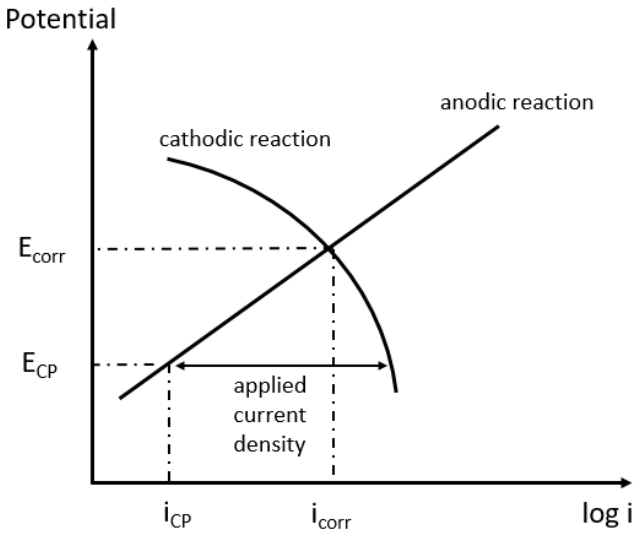


Figure 14 Cathodic protection by applied current density

The protection of hull structures made of steel is maintained by supplying a direct current from an anode through the electrolyte to bare metal surface. The potential of anode material in seawater must be more negative than the corroding surface of the metal. A corrosion cell is then established by making the bare metal surface cathode. For example, the anode is allowed to corrode, whereas the protected steel surfaces do not corrode in a cathodic protection system with sacrificial anodes [29].

Protection Criteria

According to Det Norske Veritas [30], cathodic protection is achieved for carbon and low alloy steels in seawater at potentials below -800 mV with respect to Ag/AgCl/seawater reference electrode at 25 ^{o}C. It is stated that for a correctly designed cathodic protection system, the protective potential should be in the range of -900 to -1050 mV for the main part of the design life. The potential increases towards -800 mV during the service life and eventually even less negative values towards the end of the service life. The steel is no longer protected at potentials higher than the critical as a result of poor performance of the installed anodes at the end of their service life.

When the cathodic polarization of steel surface to -800 mV (Ag/AgCl/seawater) does not reduce the corrosion rates to an acceptable limit or zero, ideally, other protection criteria should be utilized. It is stated in NACE Standard RP0193 [31] that a minimum of 100 mV cathodic polarization between carbon steel surface is sufficient.

System Design for CP

There are several fundamental considerations for a proper cathodic protection design: structure, location, protection criteria, current demand and protection method. The most important factor in cathodic protection is the structure to be protected. The information on metal including type or grade, operating conditions, dimensions, surface area, coating etc. is the starting point of a protection system. Secondly, the location of operations determines the environmental conditions including climate, water conductivity, dissolved oxygen concentration and biological activities [32].

There are two techniques of cathodic protection: sacrificial (or galvanic) anodes and impressed current [33]. CP with sacrificial anodes is an effective and more suitable method to protect bare steel surfaces of hull structures which are in direct contact with seawater. The installation of sacrificial anodes on the hull geometry is also more economical and feasible for amphibious vehicles than impressed current cathodic protection system.

Sacrificial Anodes

A sacrificial anode is a metal which corrodes instead of the protected structure in a cathodic protection system. The anode material is chosen for the protection according to galvanic series in a given medium. The galvanic series of corroding potentials of some metals and alloys relative to saturated calomel reference electrode in seawater are listed in an arranged order as seen in Figure 15. The materials having the most negative corrosion potential are placed at the bottom of the list. They are the best candidate materials for sacrificial anodes. For instance, when two materials are electrically connected in seawater, the material which is relatively at the top in the list, does not suffer from corrosion in most cases.

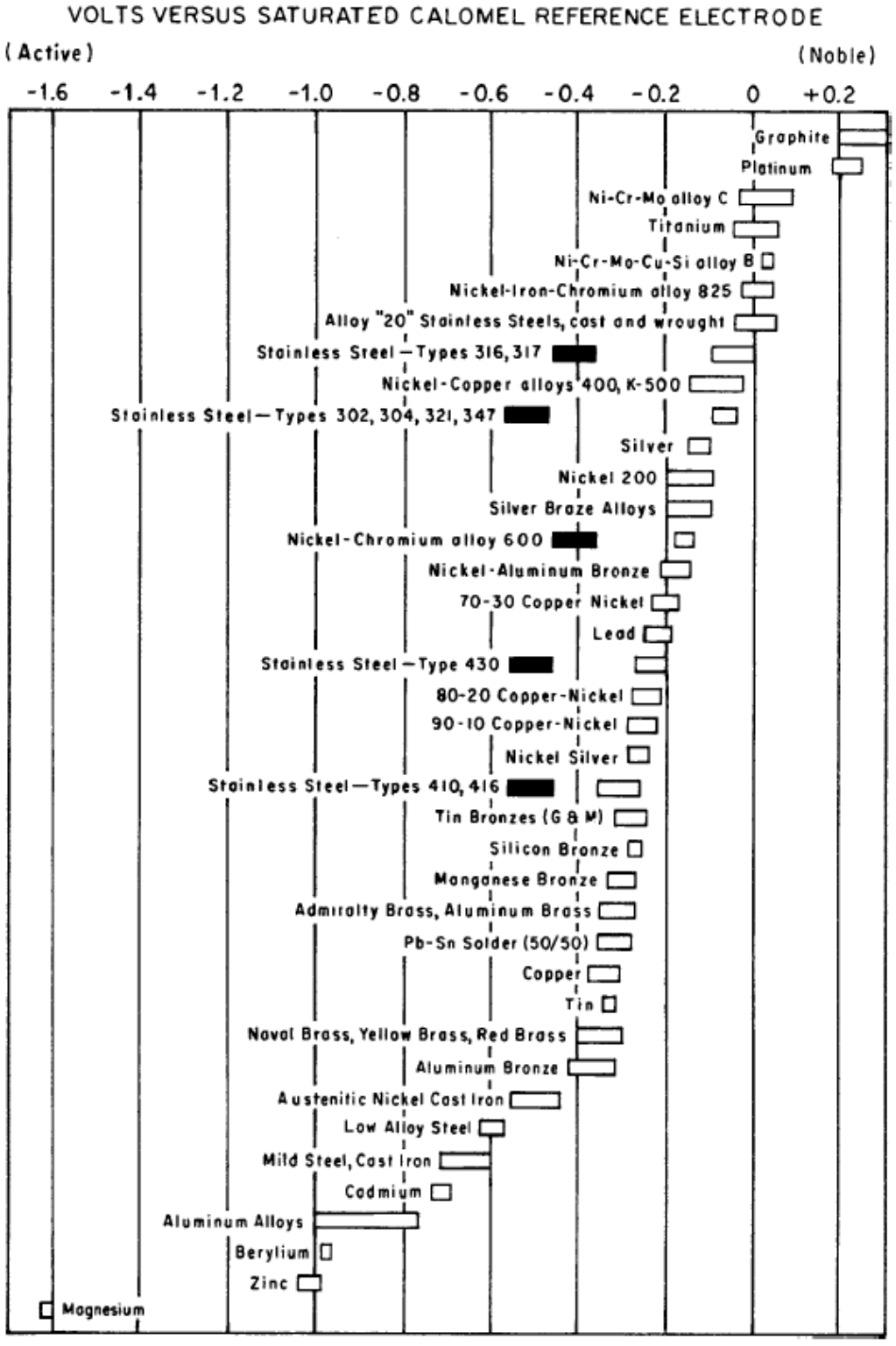


Figure 15 Galvanic series of different materials for seawater (active behavior of active-passive alloys is indicated by dark boxes) reproduced from [34]

The galvanic anode is attached to the structure to sacrifice itself so that the metal surface is protected. The cathodic protection with sacrificial anodes does not require any external power supply. The protective current is provided by the corrosion of sacrificial anode as it is more active than the surface being protected.

Current Requirement

The amount of current requirement can be determined with an actual test on existing structures using a temporary setup or a theoretical calculation based on coating efficiency [35]. The total required current (I_{req}) can be calculated as the total area of the structure (A) multiplied by the percent bare area and current density (i) [29].

$$I_{req} = A \times \%bare \times i \tag{28}$$

where current density, i, is typical current demand for cathodic protection of uncoated steel in seawater as a function of depth at subtropical environment can be estimated from the Table 1.

Table 1 Recommended current density requirement for seawater exposed uncoated metal surfaces as a function of depth at subtropical environment (12-20 ^{o}C) [30].

Depth (m)	**Initial Current density mA/m^2**	
	initial	final
0-30	170	110
>30-100	140	90
>100-300	160	110

There are several commercial sacrificial anodes available including magnesium, zinc and aluminum alloys. The energy capabilities and the consumption rates of some sacrificial anodes are given in Table 2.

Table 2 Characteristics of available sacrificial anodes [36].

Anode type	**Energy capability in A·h/kg**	**Consumption rate in kg/(A·year)**
Al-Zn-Hg	2750-2840	3.2-3.0
Al-Zn-In	1670-2400	5.2-3.6
Zinc	810	10.7
Magnesium	1100	7.9

The use of magnesium anodes is not suitable for long-term cathodic protection applications in marine environment due to the fact that magnesium anodes corrode rapidly in seawater. Magnesium anodes are usually preferred for underground applications. The anodes are surrounded by a backfill material containing gypsum, bentonite and sodium sulfate to absorb water from soil in order to keep the anodes active [29].

In seawater, anodes made of both zinc and aluminum alloys are common. Among the sacrificial anode types given above, aluminum alloy anodes are favored due to their relatively higher energy capabilities and light weight. Pure aluminum is not useful as a sacrificial anode because of its passivation characteristics. Indium in aluminum prevents the formation of oxide layer on the anode surface. The indium containing Al alloys constitute the majority of marine anodes [36,37].

The Current Output of Anode

The current output can be determined by solution resistance, the shape and the potential difference of the anode with respect to the protected metal. The resistance of an anode can be calculated with the following formulae in Table 3 according to the geometry.

Table 3 Anode resistance formulae for cathodic protection design [30]

Anode Geometry	**Resistance Formula**
Long slender stand-off L ≥ 4r	$R = \frac{\rho}{2\pi L}\left(\ln\frac{4L}{r} - 1\right)$ (29)
Short slender stand-off L < 4r	$R = \frac{\rho}{2\pi L}\left[\ln\left\{\frac{2L}{r}\left(1 + \sqrt{1 + \left(\frac{r}{2L}\right)^2}\right)\right\} + \frac{r}{2L} - \sqrt{1 + \left(\frac{r}{2L}\right)^2}\right]$ (30)
Long flush mounted L ≥ 4 · width and L ≥ 4 · thickness	$R = \frac{\rho}{2S}$ (31)
Short flush mounted, bracelet and other types	$R = \frac{0.315\rho}{\sqrt{A}}$ (32)

where R is the resistance of anode in ohms, ρ is the resistivity of electrolyte in (ohm-cm), L is the length of anode, S is the mean length of anode sides and r is the radius of anode in cm and A is the exposed surface area of anode in cm^2.

The equations (29) and (30) are valid for the condition that anodes are placed to minimum distance of 30 cm from the protected metal [30].

Ohm's law can be used to calculate the current output, I, for a single anode.

$$I = \frac{V}{R} \tag{33}$$

where V is the difference between the selected protection potential of the steel and the closed-circuit potential of the anode.

Then, the number of anodes (N) required for a system can be estimated by combining the equations (28) and (33).

$$N = \frac{Total\ current\ demand}{Current\ output\ per\ anode} \tag{34}$$

The distribution of anodes in the system is as important as the quantity. The distance between the anodes should be adjusted to provide the sufficient current to the critical parts of the protected assembly during installation.

2.7 Numerical Modeling

Computer modeling is quite useful in solving electrochemical problems. Numerical analysis enables to get valuable information about potential and current distributions on corrosion behavior of metals in corrosive medium. The electrochemical theory behind the modeling is briefly mentioned below.

Theory [13]

The flux of a solute species in dilute solutions is given by Nernst-Plank equation to describe the movement of charged species in terms of migration in an electric field, diffusion in a concentration gradient, and convection with the fluid velocity.

$$N_i = -z_i u_i F c_i \nabla \phi - D_i \nabla c_i + v c_i \tag{35}$$

where N_i is the flux density, in moles per square centimeter; z_i is the number of proton charges carried by ion I; u_i is the average velocity and c_i is the concentration of ionic species I in the electrolyte; ϕ is the electrostatic local potential of the electrolyte; D_i is the diffusion coefficient of species I and v is the average velocity of the electrolyte.

The motion of charged particles creates current in the electrolyte. The local current density, *i*, can be expressed in amperes per square centimeter.

$$i = F \sum_i z_i N_i \tag{36}$$

where $z_i F$ is the charge per mole.

The current density expression in the electrolyte can be expanded using the terms in the flux equation as;

$$i = -F^2 \nabla \phi \sum_i z_i^2 \, u_i c_i - F \sum_i z_i \, D_i \nabla c_i + Fv \sum_i z_i \, c_i \tag{37}$$

The last term in the above equation becomes zero due to the electroneutrality since fluid motion without charge density is not contributing to the current density. Moreover, by considering that there is no concentration gradient in the electrolyte, the second term can also be removed from the equation. The current density expression is then reduced to;

$$i = -\sigma \nabla \phi \tag{38}$$

where σ is the conductivity of the electrolyte and expressed as;

$$\sigma = F^2 \sum_i z_i^2 \, u_i c_i \tag{39}$$

Material balance for a small-volume element can be expressed by the differential conservation law.

$$\frac{\partial c_i}{\partial t} = -\nabla \cdot N_i + R_i \tag{40}$$

The term on the left represents the accumulation which is the rate of the change of concentration due to the differences in the fluxes of a small-volume element. The accumulation is equal to net input ($-\nabla \cdot N_i$) plus production (R_i) in homogeneous chemical reactions in the bulk solution.

Multiplying equation (40) by $z_i F$ and adding over species yield;

$$\frac{\partial}{\partial t} F \sum_i z_i c_i = -\nabla \cdot F \sum_i z_i N_i + F \sum_i z_i R_i \tag{41}$$

Since the reactions are occurring on the surface of the electrodes, the bulk reaction term R_i is often zero. Electroneutrality except in the diffuse part of the double layer in the electrolyte can be expressed as;

$$\sum_i z_i c_i = 0 \tag{42}$$

The equation (41) with the assumption of electroneutrality can be reduced to;

$$\nabla \cdot i = 0 \tag{43}$$

Insertion of the equation (38) into the equation (43) yields;

$$\nabla \cdot (\sigma \nabla \phi) = 0 \tag{44}$$

When the conductivity is constant in the electrolyte;

$$\nabla^2 \phi = 0 \tag{45}$$

This indicates that the potential satisfies Laplace's equation in a region of homogenous composition [13].

In numerical analysis, the model is discretized in elements of different shapes and sizes according to the physics used in simulation and the geometry of the interface between the electrode and electrolyte. The Laplace equation (45) is solved for finite elements created by dividing the domain and the surface of the representative geometry into small elements which are linked by nodes in a complete mesh. The potential distribution is resulted from the solution of the Laplace equation and the respective boundary conditions which are prescribed potential, prescribed current density and nonlinear relation between the potential and current density [38].

CHAPTER 3

EXPERIMENTAL STUDY

Electrochemical testing methods have been extensively used for studying fundamentals of corrosion reactions in various environments. Corrosion, as an electrochemical process, occurs at the interface of a metal and its surrounding environment. In this degradation process, the current flows from anodes or anodic areas on the surface of the metal to cathodes or cathodic areas of the metal surface through the surrounding medium. The corrosion current cannot be measured directly so that an inert electrode and an external electrical circuit are attached to the corrosion cell. Polarization is the potential deviation of an electrode from its equilibrium value due to a net flow of current through the electrode [39].

3.1 Materials

The corrosion behavior of several steel grades in artificial seawater was investigated in this study. Hull structures of the amphibious vehicle are made of these grades of steels. Chemical compositions of all steel samples used in this study are given in Table 4. Samples were cut from steel bars which were provided by FNSS Defence Systems Co. Inc.

Table 4 Chemical compositions of selected steels.

Steel	**C %**	**Mn%**	**P%**	**S%**	**Si%**	**Cr%**	**Mo%**
S355 JR*	0.27	1.7	0.030	0.045	0.60	-	-
AISI 1010	0.08-0.13	0.3-0.6	0.030	0.050	0.07-0.60	-	-
AISI 4140	0.38-0.43	0.75-1.00	0.035	0.040	0.15-0.35	0.8-1.1	0.15-0.25

*maximum limits for a typical S355 structural steel

Sample Preparation

Prior to electrochemical tests, each steel sample surface was ground with P80 and P600 grade sand papers. Samples were washed with distilled water to remove any contaminants and then rinsed in acetone. Only bottom surfaces of steel bars were left open, the rest was isolated by tape to define electrode-electrolyte interface.

3.2 Electrolyte

Artificial seawater was prepared in accordance with the ASTM D1141-98, standard practice for preparation to substitute ocean water, as electrolyte solution for laboratory corrosion tests [40]. Two stock solutions consisting of different salts were prepared (see Table A-1 in APPENDIX I). Majority of the first stock solution was $MgCl_2.6H_2O$. Anhydrous $CaCl_2$ and $SrCl_2.6H_2O$ were also present in the first solution. Second stock solution was prepared by dissolving KCl, $NaHCO_3$, KBr, H_3BO_3 and NaF. The stock solutions were stored in amber containers. To prepare substitute seawater prior to use, NaCl and anhydrous Na_2SO_4 were dissolved in water then specified amounts of two stock solutions were added. The constituents and concentrations of salts in the solution used for artificial seawater are shown in Table 5. Finally, the pH of the artificial seawater was adjusted to 8.2 with 0.1 N NaOH solution.

Table 5 Artificial seawater constituents and concentrations.

Compound	Concentration g/L
NaCl	24.53
$MgCl_2$	5.20
Na_2SO_4	4.09
$CaCl_2$	1.16
KCl	0.695
$NaHCO_3$	0.201
KBr	0.101
H_3BO_3	0.027
$SrCl_2$	0.025
NaF	0.003

3.3 Reference Electrode

Saturated calomel electrode (SCE) was preferred for this study. It is a type of a mercury reference electrode based on the equilibrium between Hg and Hg_2Cl_2. As seen in Figure 16, a paste containing Hg and Hg_2Cl_2 and KCl solution in a small container was placed in a glass tube filled with KCl solution that has a porous salt bridge to permit electrons to flow in a glass [40,41]. This reference electrode provides 241 mV potential relative to standard hydrogen electrode (SHE).

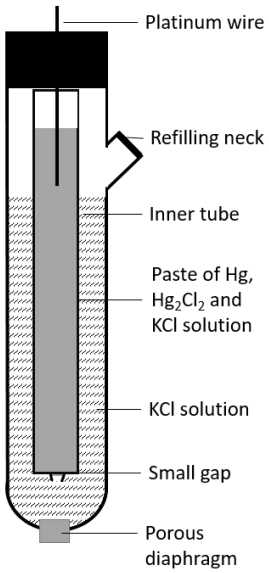


Figure 16 A typical construction of a calomel electrode

3.4 Experimental Setup

Corrosion cell was established in a three-necked glass vessel. The vessel was filled with artificial seawater. Metal sample as working electrode was placed through the middle opening. Graphite as the counter electrode and saturated calomel electrode (SCE) as reference electrode were selected and placed through the remaining openings to complete the cell as seen in Figure 17. All electrodes were connected via assigned cables to Gamry Refence 3000 Potentiostat. The data acquisition was

managed by Gamry Framework software which was installed to a computer connected to the potentiostat.

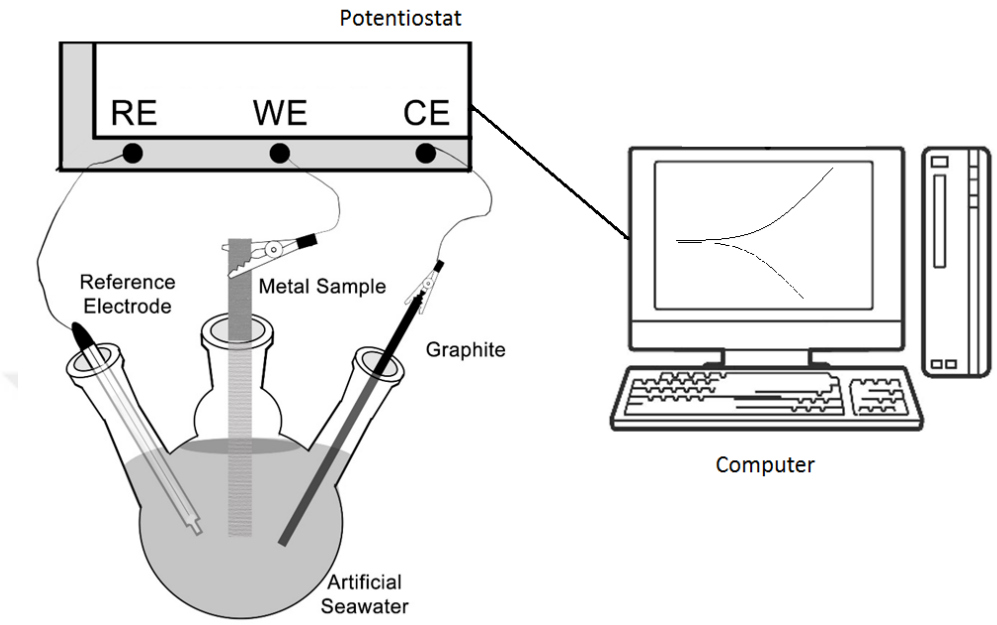


Figure 17 A schematic of the corrosion cell setup together with the potentiostat

Tafel scan analysis was conducted for each steel sample. The current response was measured as a function of potential which was swept by the potentiostat. The initial and final potentials were defined so as the open circuit potential would be at the middle of the scanning path (-0.25 to +0.25 V). The scanning rate was set to 1 mV/s. All electrochemical tests were implemented at room temperature.

Potentiodynamic polarization curves were plotted by a computer data acquisition system. Potential and current measurements were obtained by multichannel analog to digital converter which monitors the potential and current outputs from the potentiostat. Real time polarization curves were drawn by utilizing computer graphic capabilities and scaled on the monitor screen.

CHAPTER 4

RESULTS AND DISCUSSION

4.1 Electrochemical Tests

The polarization responses obtained for S355 JR, AISI 1010 and AISI 4140 steels in artificial seawater at 20°C are presented in Figure 18, Figure 19 and Figure 20, respectively. As expected, experimentally derived curves were not linear near the corrosion potential due to the interference from the anodic and cathodic reactions in the region [39]. The regions away from the corrosion potential were nearly linear before curves deviate due to excess polarizations. In this region, namely Tafel region, anodic and cathodic slopes are constant.

The electrochemical parameters including corrosion current density (i_{corr}), corrosion potential (E_{corr}), anodic and cathodic Tafel slopes (β_A and β_C) were obtained from the extrapolation of the anodic and cathodic branches of each Tafel plot. The potentiodynamic data were interpreted via the Tafel fit command in Gamry eChem software [43]. The software uses a non-linear chi squared minimization to fit the experimental data in selected Tafel region to the Butler-Volmer equation. The goodness of fit was verified by the chi-square parameter. Reasonably good curve-fittings were obtained with chi-square values varied from 112.6×10^{-3} to 576.3×10^{-3}. The arithmetic mean of the electrochemical parameters with standard deviation values (S_R) are given in Table 6.

Table 6 The overall mean results of electrochemical polarization tests in artificial seawater at 20°C

Steel	**β_A (mV/decade)**	***S_R***	**β_C (mV/decade)**	***S_R***	**i_{corr} (μA/cm^2)**	***S_R***	**E_{corr} (mV)**	***S_R***
S355 JR	115.4	*8.334*	289.3	*14.811*	26.20	*4.315*	-667	*7.409*
AISI 1010	99.2	*0.712*	179.2	*12.634*	24.53	*0.094*	-696	*13.441*
AISI 4140	74.3	*2.061*	230.0	*15.864*	16.57	*0.450*	-743	*2.449*

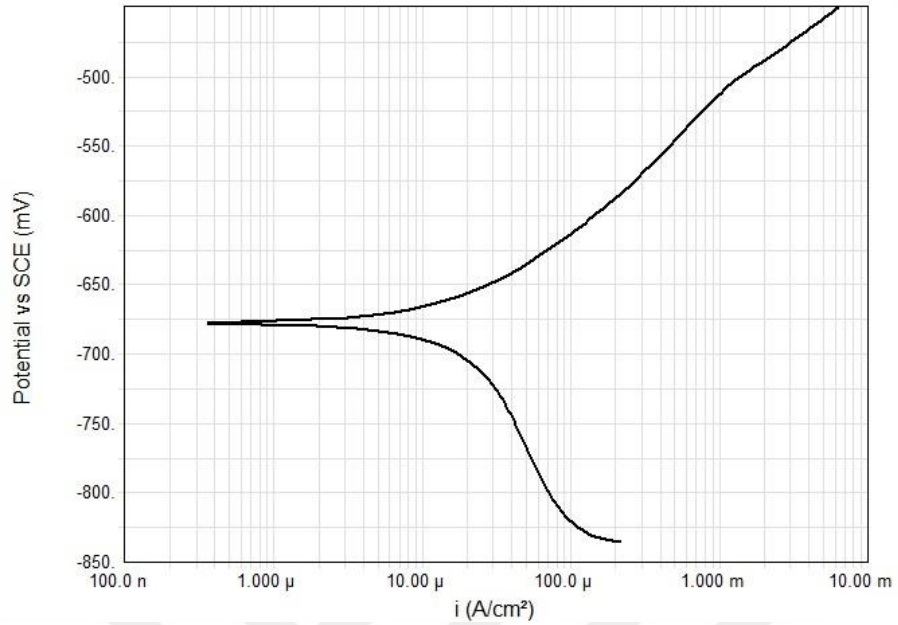


Figure 18 Potentiodynamic polarization curve for S355 JR in artificial seawater at 20 ^{o}C

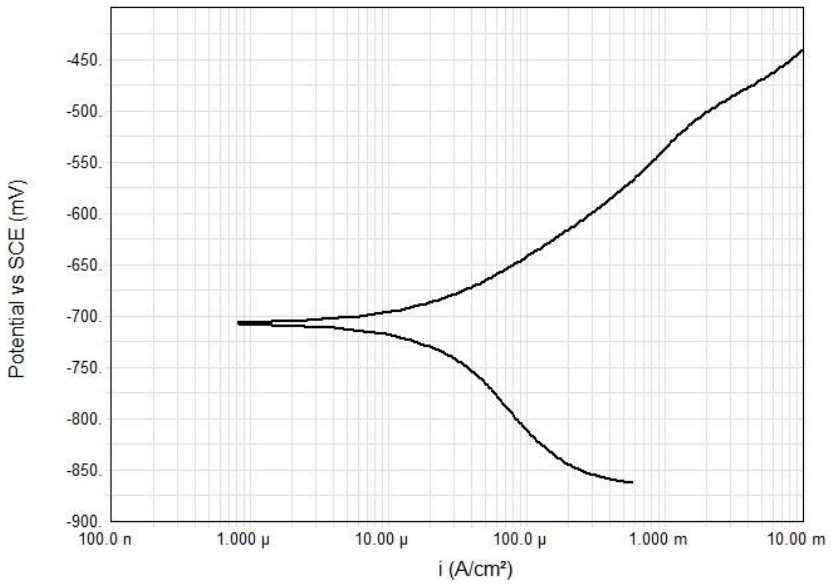


Figure 19 Potentiodynamic polarization curve for AISI 1010 in artificial seawater at 20 ^{o}C

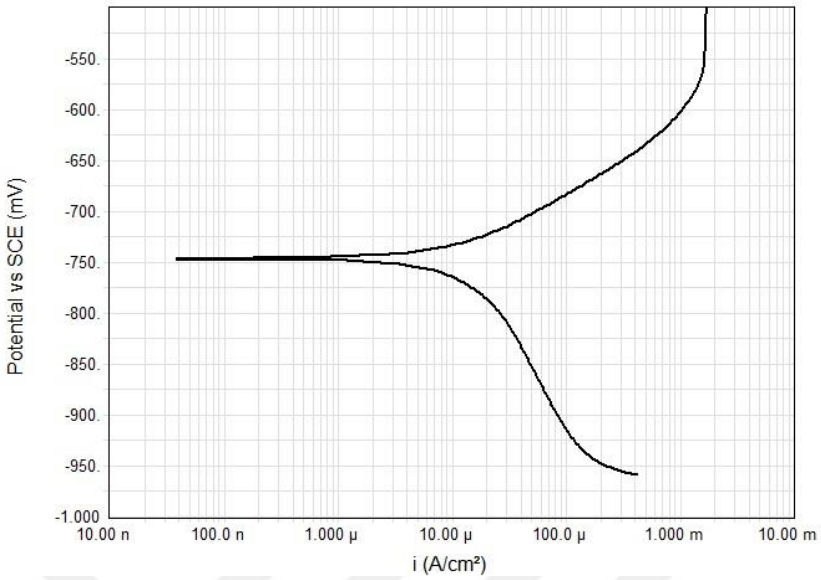


Figure 20 Potentiodynamic polarization curve for AISI 4140 in artificial seawater at 20 ºC

To illustrate the Tafel extrapolation method, it was applied manually to one of the polarization curves for AISI 4140 as seen in Figure 21. The anodic and cathodic Tafel slopes were drawn on the polarization curves. The exchange current density value corresponds to the intersection of the anodic and the cathodic extrapolated slopes was determined. Nearly the same parameters were obtained by manual Tafel extrapolation when compared to the Tafel fit routine of Gamry eChem software.

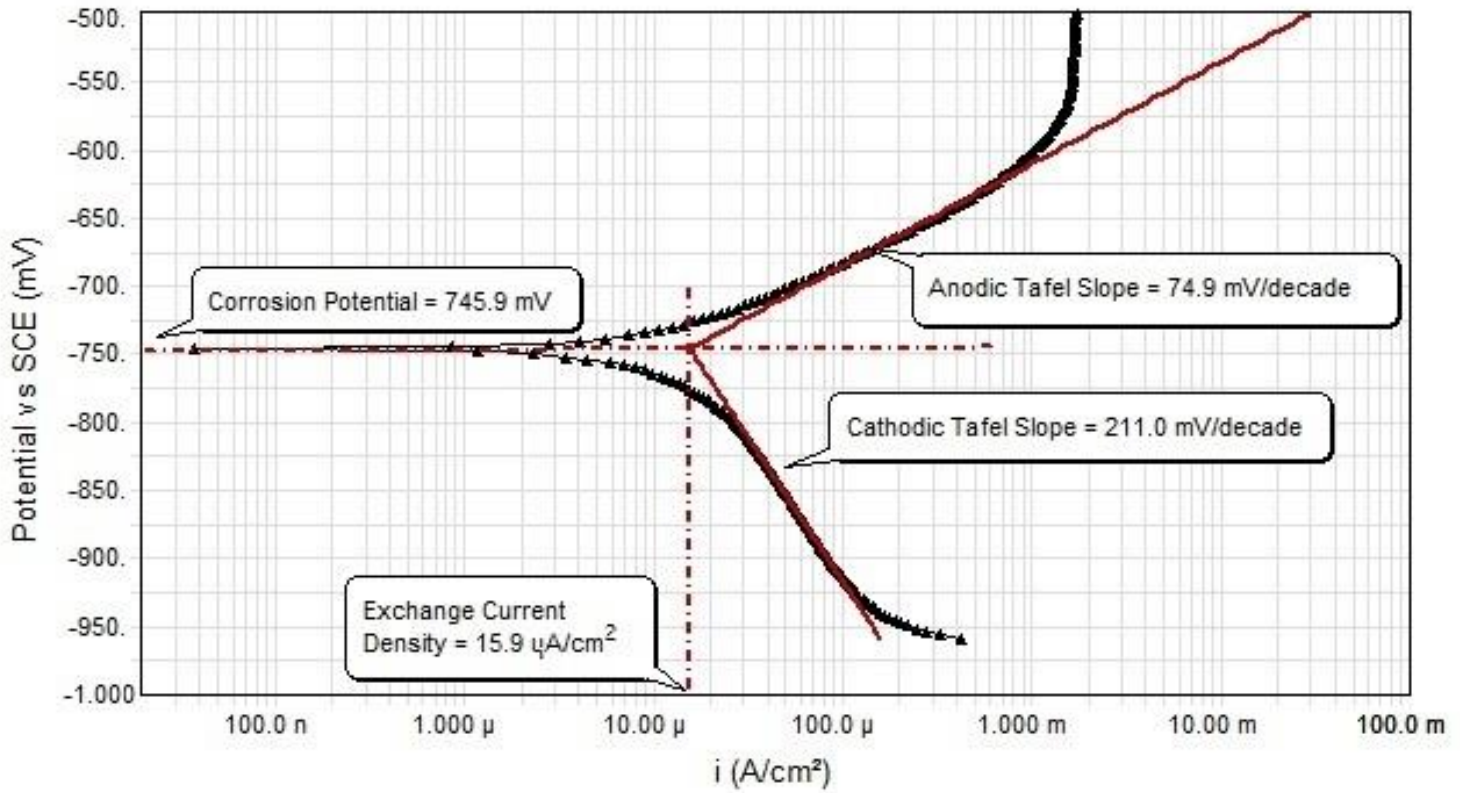


Figure 21 The Tafel extrapolation method applied manually to AISI 4140

In the Tafel fit analysis by Gamry eChem, the corrosion reactions were assumed to be under kinetic control. The effect of concentration polarization could not be evaluated from the fit routine. However, the limiting current density (i_L) due to the diffusion controlled mixed corrosion reactions should be introduced to the model for better cathodic protection simulation.

It can be said that the reason for the cathodic polarization was due to the combined effects of oxygen reduction and hydrogen evolution reactions on the steel surfaces. As mentioned in previous chapters, the transport of dissolved oxygen molecules through to the diffusion layer from the bulk solution limited the rate of corrosion up to a certain current density. Thereafter, the cathodic reaction was dominated by hydrogen evolution reaction. The limiting current plateau on the Tafel plots given above was not well defined.

The limiting current density is a critical parameter for the cathodic reactions in corrosion process under diffusion control. As suggested by Ponce de Leon et al [44], there are four strategies to determine the limiting current values from the Tafel plots: direct measurements from potential-current curves, estimation from the current value at the middle of the limiting current plateau, evaluation of the first derivate *dI/dE* in the polarization curve and from the plots of *E/I* against the inverse of current.

4.1.1 Determination of Limiting Current Densities

As illustrated in Figure 22, a specific region on the cathodic branch of the polarization curve of AISI 4140 was examined for determination of the limiting current density. The derivative of current density with respect to the potential (di/dE) was plotted against the applied potential (see Figure 23). The ill-defined plateau might be resulted from the combined effects of two cathodic reactions: hydrogen evolution and oxygen reduction.

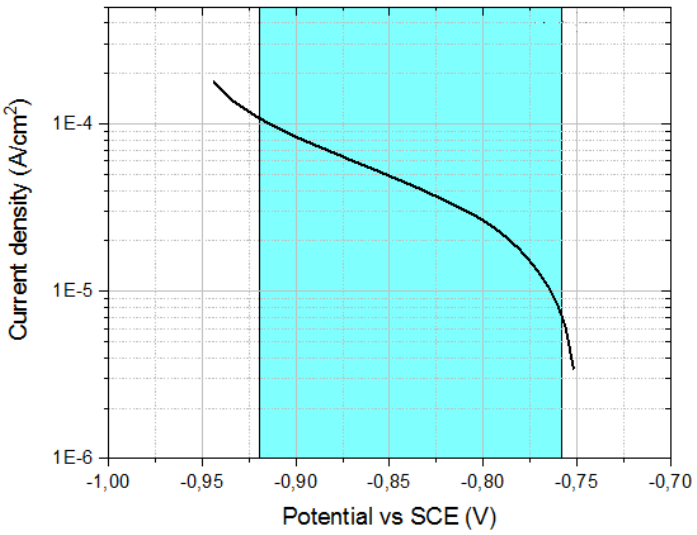


Figure 22 The cathodic branch and the limiting current plateau of Tafel plot of AISI 4140

The evaluation of the plot revealed the limiting current density which is the closest point to zero di/dE slope as seen in Figure 23. The limiting current density was found as 32.0×10^{-6} A/cm^2 for AISI 4140 steel from the turning point of i vs. E graph.

The same procedure was followed for the other grades of steel in this study. The overall limiting current density values derived by the first derivative method are given in Table 7.

Table 7 The limiting current density values derived from the Tafel plots

Steel	**i_L (µA/cm^2)**	**E_L (mV)**
S355 JR	67.1	-750
AISI 1010	49.0	-768
AISI 4140	32.0	-814

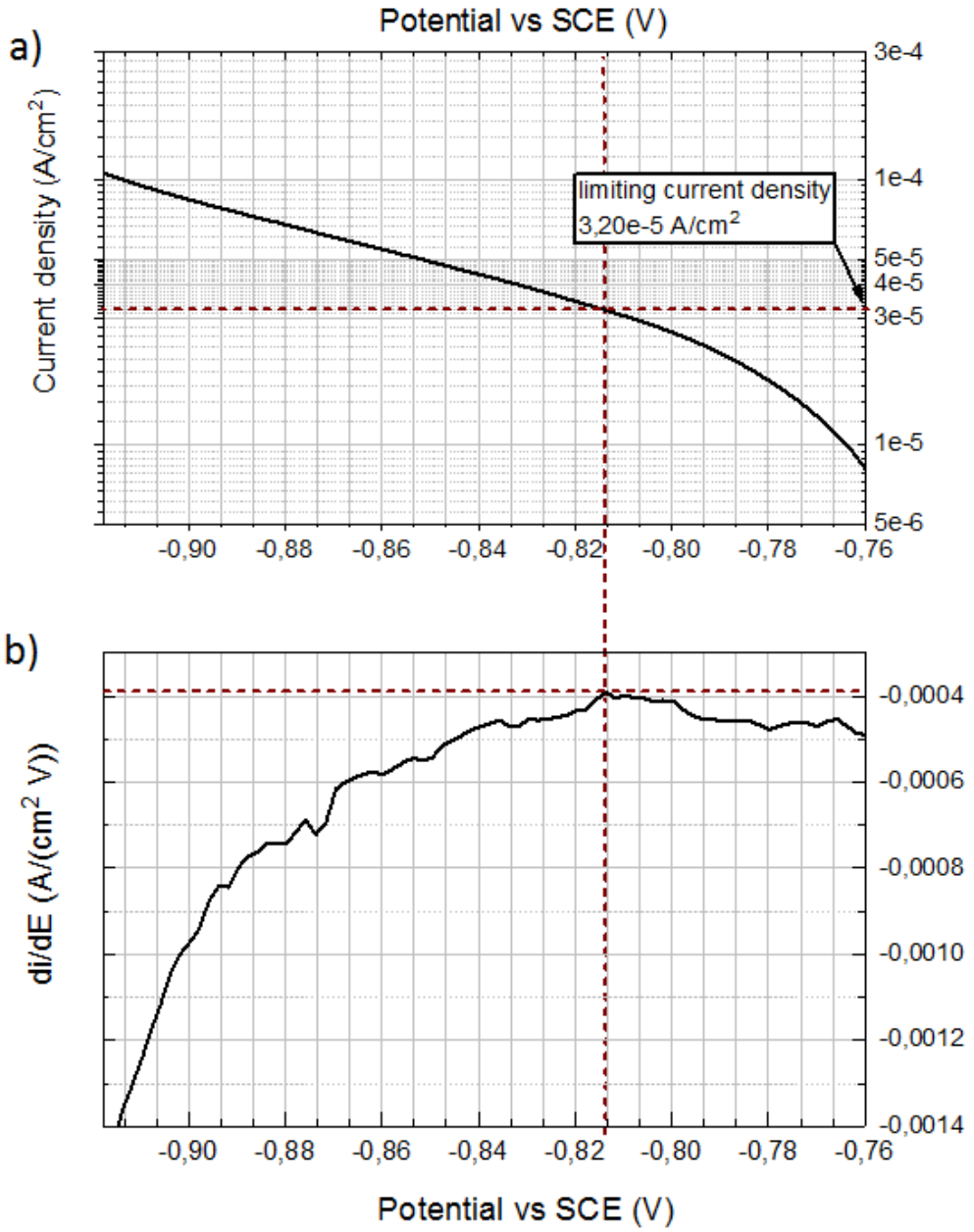


Figure 23 Determination of the limiting current density value by the derivative method for AISI 4140. The specific region on the cathodic branch of the polarization curve (a) and the first derivate di/dE of the polarization curve (b) are used.

4.2 Numerical Modeling

Numerical modeling of cathodic protection with sacrificial anodes was investigated in this part. Corrosion reactions and resulting potential distributions at metal-electrolyte interface were analyzed by finite element method (FEM). The vehicle geometry was divided into small elements to numerically describe the geometry in this method. Governing equations and boundary conditions were identified. Discretized equations were solved using mathematical routines. Computations were performed through COMSOL Multiphysics 5.2 software.

The protection potential for the uncoated steel surfaces of the hull structures was maintained by the polarization with Al-Zn-In sacrificial anodes placed on proper locations of the vehicle body in this study. In the following modeling applications, the properties of only AISI 4140 were assigned to bare steel surfaces. The surface areas of other steel types were not accounting much to alter the modeling, because they were the types used for bots, nuts, washers etc.

4.2.1 Model Geometry

The quarter part of the vehicle geometry consisting of several steel structures is shown in Figure 24. Full geometry of the amphibious vehicle consisting of the steel hull structures used in this study is given in APPENDIX II.

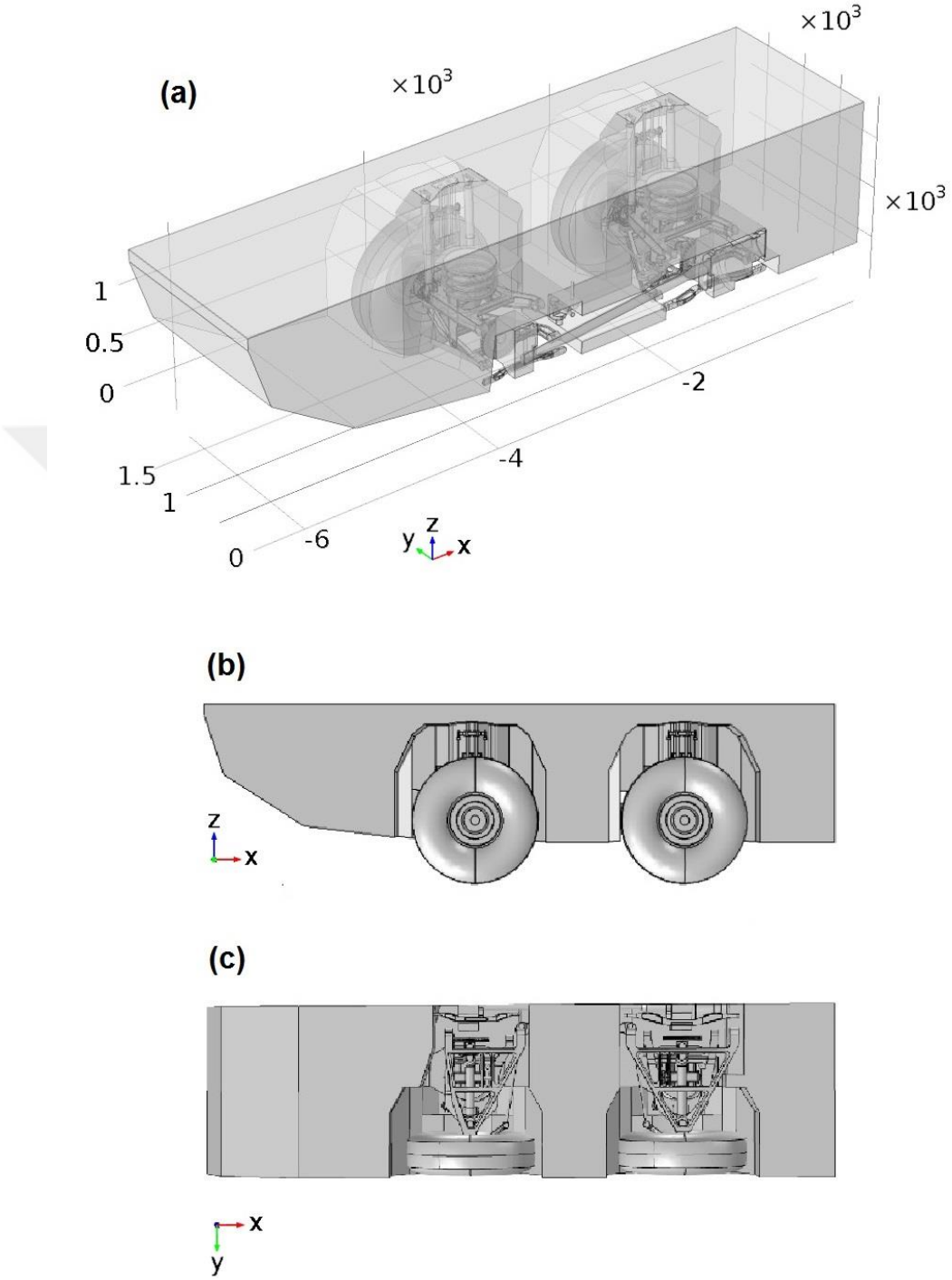


Figure 24 The quarter part of the vehicle geometry, (a) isometric transparent view with dimensions in 10^3 mm, (b) side view, (c) bottom view

4.2.2 Cathodic Protection Design

Cathodic protection system was designed for the steel hull structures, made of AISI 4140, in seawater. The number and locations of sacrificial anodes in a system depend on the geometry and total area of the structure to be protected. In this modeling study, a cathodic protection design was made for the highlighted steel components in Figure 25. The total surface area of the components for the selected quarter was measured as 13.41 m^2 from the model geometry.

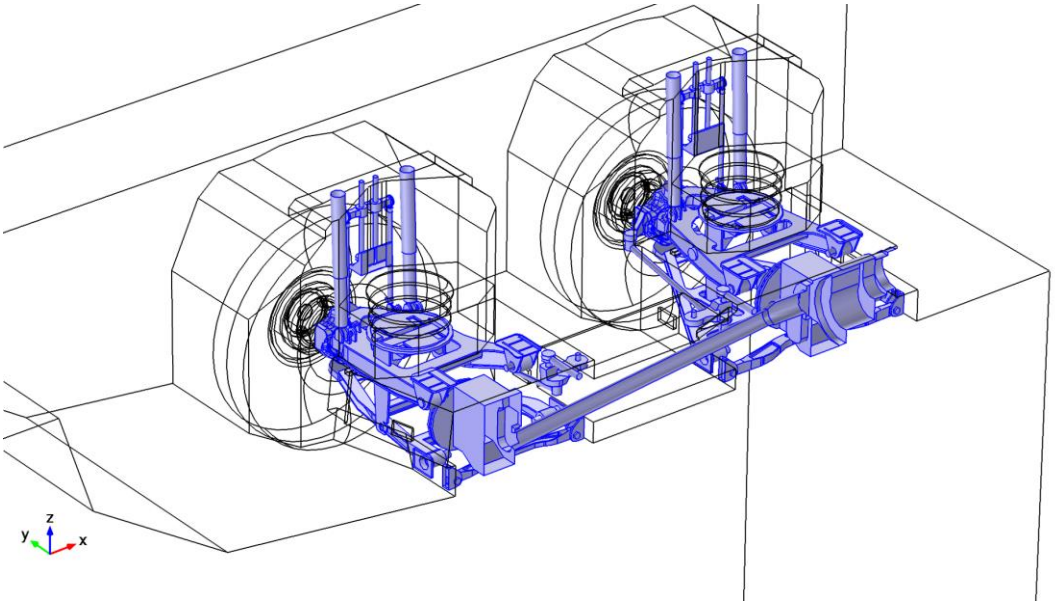


Figure 25 Steel components of the selected quarter of the hull structure

The protection potential and corresponding current density demand for uncoated steel surfaces in seawater were determined by extrapolating the anodic Tafel slope on the polarization diagram to the selected potentials (-790 and -843 mV relative to SCE) as seen in Figure 26.

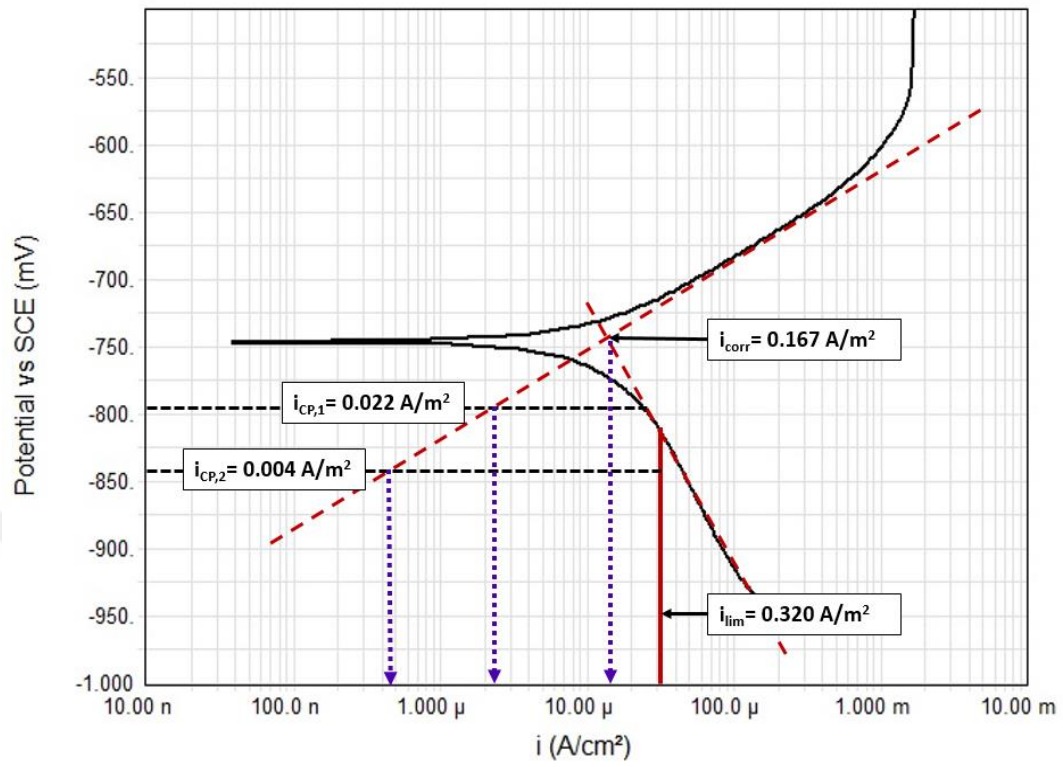


Figure 26 Polarization of AISI 4140 to the different protection potentials

The two conventional protection criteria (see chapter 2) were compared in terms of corrosion rates, CR. Faraday's Law [45] was used to calculated the uniform rates of corrosion in terms of penetration in mm/year as seen in Table 8.

$$\mathrm{CR} = 327.2\frac{i_{corr} \cdot EW}{\rho} \tag{46}$$

where the equivalent weight, EW (=27.92), was calculated by dividing the atomic weight of the iron (=55.84) to the number of electrons (=2) required to oxidize a typical carbon steel. The density of steel, ρ, was taken as 7800 kg/m^3. The value 327.2 was calculated by taking the ratio of one year in seconds to Faraday's constant.

Table 8 Resultant corrosion rates according the cathodic polarization

	Corrosion potential (mV)	Current density (A/m^2)	Corrosion rate (mm/y)
without CP	-743	0.167	0,196
CP,1	-790	0.022	0,026
CP,2	-843	0.004	0,005

The significantly lower corrosion penetration rate was obtained when the equilibrium potential is shifted by 100 mV in the negative direction. Therefore, the protection potential value for the cathodic protection designed for this study was selected as -843 mV.

The required current density for shifting the potential to -843 mV was determined as 0.316 A/m^2 from Figure 26. This is the difference between the limiting current density and the corrosion current density when protection is applied. The total current required for the protection of total steel surface area of 13.41 m^2 was calculated using equation (28).

$I_{req} = 13.41\ m^2\ x\ 0.316\ A/m^2$

$I_{req} = 4.238\ A$

Parameters of the sacrificial anodes for the cathodic protection system are given in Table 9. The indium activated aluminum alloy anodes were preferred for this application. As being the predominant marine aluminum anode, this type of anodes can be used for variety of offshore applications. The performance of commercially available indium containing aluminum anodes (Coral® “A” High Grade by Skarpenord and Galvanum® III by CP Tech) in seawater was utilized. Accordingly, the closed-circuit potential of indium activated sacrificial anodes was taken as -1080 mV with respect to SCE. The chemical compositions and performance data of the selected anode are given in Table A-2 and Table A-3 in APPENDIX I.

Table 9 Anode parameters and seawater resistivity in CP system

Seawater resistivity	0.2 Ω·m
Anode potential	-1080 mV
Anode length	135 mm
Anode width	70 mm
Anode thickness	22 mm
Anode surface area	18470 mm^2

The dimensions of the anodes were initially determined by the manufacturer of the amphibious vehicle. Nevertheless, it was possible to support the protection system with additional anodes having various shapes.

The anode resistance was calculated using equation (32). One of the large surfaces of the anode was excluded from the total area calculation since the anode was attached to the vehicle body by this face.

$$R = \frac{0.315\ x\ 0.2\ \Omega \cdot m}{\sqrt{0.01847\ m^2}}$$

$$R = 0.464\ \Omega$$

The current output per anode was calculated using equation (33).

$$I = \frac{-0.843\ V - (-1.080\ V)}{0.464\ \Omega}$$

$$I = 0.511\ A$$

The quantity of sacrificial anodes was then estimated from equation (34) by dividing the required total current to the current output of a single anode.

$$N = \frac{4.238}{0.511} = 8.293 \cong 8$$

The number of anodes required for the cathodic protection of given dimensions was estimated as 8.

Assumptions

Before establishing a model for cathodic protection of the bare steel surfaces, several assumptions were made to ease the computations:

- The corrosion on the bare steel surfaces was uniform. Pitting or filiform corrosion under the coating layer were not included to the model.
- The hull structures were made of only a single type of material. Although aluminum alloy plates were used in the body of the amphibious vehicle, the galvanic interactions were not studied. Furthermore, they are going to be modeled separately.
- The electrolyte composition was homogenous near the boundaries. The effect of diffusion of dissolved oxygen in seawater was not directly included to the model. The limiting current density was calculated from the polarization and introduced into the governing equation as a kinetic parameter.
- The model geometry was consisting of large structural components. Small machine elements such as bolts, screws, nuts etc. and washers were excluded from the geometry.

Boundary Conditions and Governing Equations

Corrosion reactions occur on the boundaries between electrode surfaces and seawater. Boundary conditions in numerical modeling were used to simulate the current and potential relations on the surfaces of uncoated steel.

Anode Boundaries

Al-Zn-In alloy was selected as sacrificial anode in the modeling. This type of aluminum alloy is generally used for cathodic protection systems in offshore structures. The polarization of the alloy in its activated state is very low so that the surface potential in seawater was fixed to constant value which was the closed-circuit potential in the protection system.

Bare Steel Boundaries

There were three electrochemical reactions that may occur on the bare steel boundaries depending on the polarization direction: iron dissolution as anodic reaction, both hydrogen evolution and oxygen reduction reactions as cathodic reactions.

Boundary conditions on the uncoated surfaces are affected by polarization of the electrodes. Potential deviates from the equilibrium value on the surface of bare steel components due to the electrochemical interactions. The surface over-potential is denoted by η and expressed as

$$\eta = V - \phi \tag{47}$$

The resulting boundary condition at the bare steel surfaces has a nonlinear relation between the potential and the potential derivative.

It can be stated that the current density is a function of the surface over-potential

$$i = f(\eta) \tag{48}$$

Seawater near the bare steel surfaces is not an equipotential surface due to the electrode kinetics. The result of calculations involving surface over-potential is called secondary current distribution.

The current density depends exponentially on the surface over-potential. This relation can be expressed by the Butler-Volmer equation.

$$i = i_0 \left[e^{\left(\frac{\alpha_a F}{RT}\eta\right)} - e^{\left(\frac{\alpha_c F}{RT}\eta\right)} \right] \tag{49}$$

where i_0 is the exchange current density which depends on the composition of the seawater, temperature and the nature of the electrode surface. Both α_a and α_c are Tafel constants which are derived from the slopes of anodic and cathodic branches of the Tafel plot.

The limiting current density, i_{lim}, on the local surfaces of the bare steel can be introduced into the model by the assumption of a diffusion layer at the steel surface. Local current density, i_{local}, can be calculated from the equation given below when mass transport of ionic species is included explicitly in the model [46].

$$i_{local} = \frac{i}{1 + \left\| \frac{i}{i_{lim}} \right\|} \tag{50}$$

where i is the current density when mass transport of the ionic species is limited.

The Tafel slopes for anodic (β_a) and cathodic (β_c) reactions from the polarization curves depend on the transfer coefficients and they can be written as;

$$\beta_a = \frac{2.303\ RT}{\alpha_a F} \tag{51}$$

and

$$\beta_c = \frac{2.303\ RT}{\alpha_c F} \tag{52}$$

The coated surfaces of the steel components were defined as isolated boundaries and the potentials on the normal of the boundaries are zero.

$$\frac{\partial \phi}{\partial n} = 0 \tag{53}$$

Boundary conditions of the cathodic protection model are illustrated in Figure 27.

Since the secondary current distribution is valid for most electrochemical systems, cathodic protection of a metal can be simulated by considering kinetic irreversibility on non-isolated boundaries.

The electrochemical parameters obtained from laboratory tests are given in Table 10. The steel surface in this example model was made of only AISI 4140.

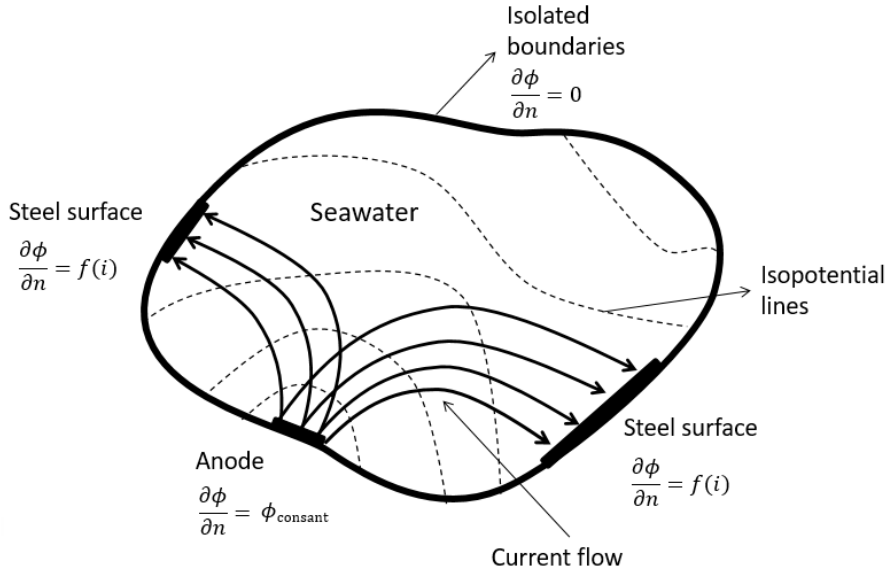


Figure 27 Boundary conditions for cathodic protection model

Table 10 Overall parameters of corrosion kinetics used in modeling

Parameter	**Value**	**Description**
σ_l	5 S/m	Seawater conductivity
$E_{corr,4140}$	-0.743 V	Corrosion potential of AISI 4140
$i_{corr,4140}$	0.1657 A/m^2	Corrosion current density of AISI 4140
$i_{lim,4140}$	0.32 A/m^2	Limiting current density of AISI 4140
$\beta_{a,4140}$	74.3 mV/decade	Anodic Tafel slope of AISI 4140
$\beta_{c,4140}$	230 mV/decade	Cathodic Tafel slope of AISI 4140
$\alpha_{a,4140}$*	0.7824	Anodic Tafel constant of AISI 4140
$\alpha_{a,4140}$*	0.2528	Cathodic Tafel constant of AISI 4140

*The Tafel constants were calculated using equations (51) and (52)

4.2.3 Meshing the Model Geometry

Meshing the model geometry is essential for simulation processes because the finite element method is applied to the model geometry by diving it into small elements for approximation. COMSOL Multiphysics allows three kinds of meshes: tetrahedral, hexahedral and prismatic. In general, solid bodies in three dimensions can be meshed with tetrahedral elements which are the default element type for most physics in the software [47]. Tetrahedral element type was chosen for meshing the hull structures and surrounding medium in this study (see Figure 28).

There are several pre-defined element size options ranging from extremely fine to extremely coarse as physics-controlled mesh. Instead of using pre-defined parameter sets, building a custom mesh was more appropriate for this study.

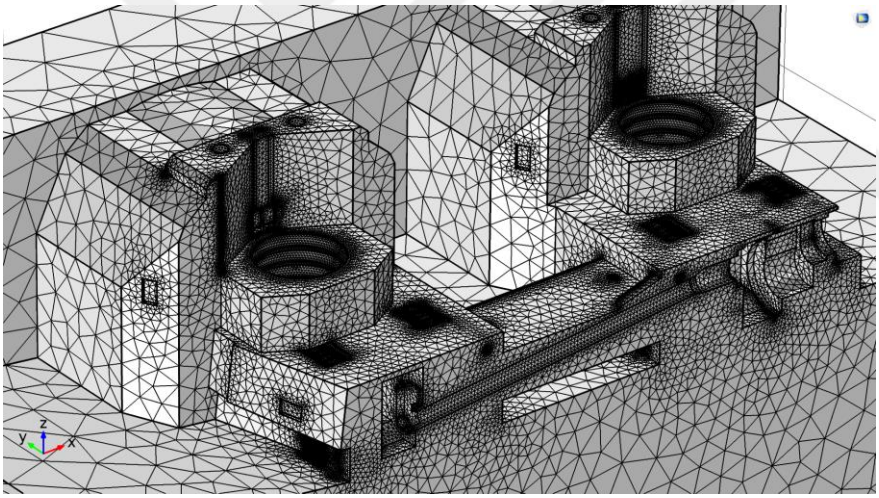


Figure 28 Meshed model geometry

Creation of tetrahedral meshes results triangular elements on the boundaries, edge elements on the edges and vertex elements on the interception of edges or planes. The detailed report of the mesh elements is given in Figure 29.

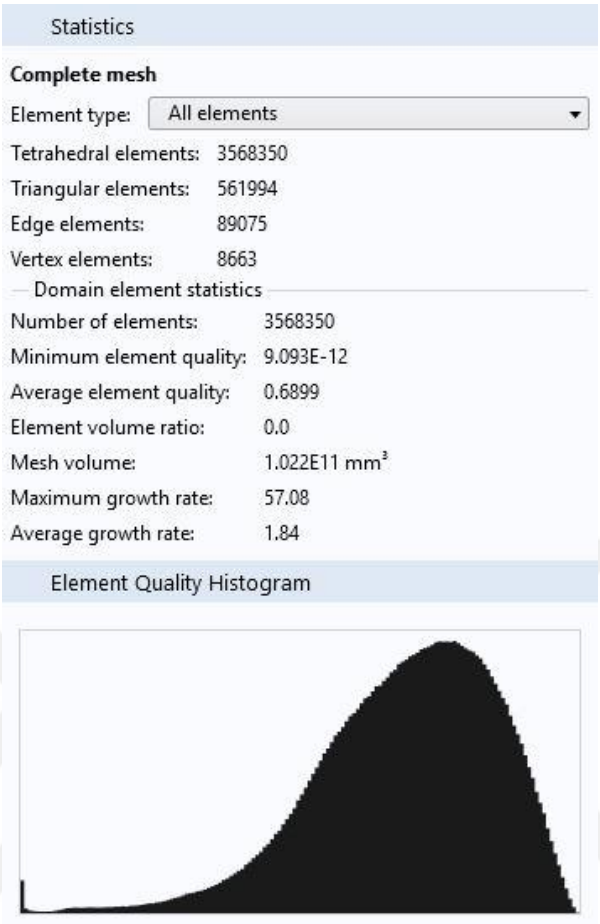


Figure 29 Statistics on mesh quality

A left-skewed element quality histogram given at the bottom of Figure 29 is considered as a good indicative of an average element quality and number of elements. The quality depends on the five mesh parameters: maximum element size, minimum element size, maximum element growth rate, curvature factor and resolution of narrow regions [48]. The custom mesh parameters modified for this study is given in Figure 30.

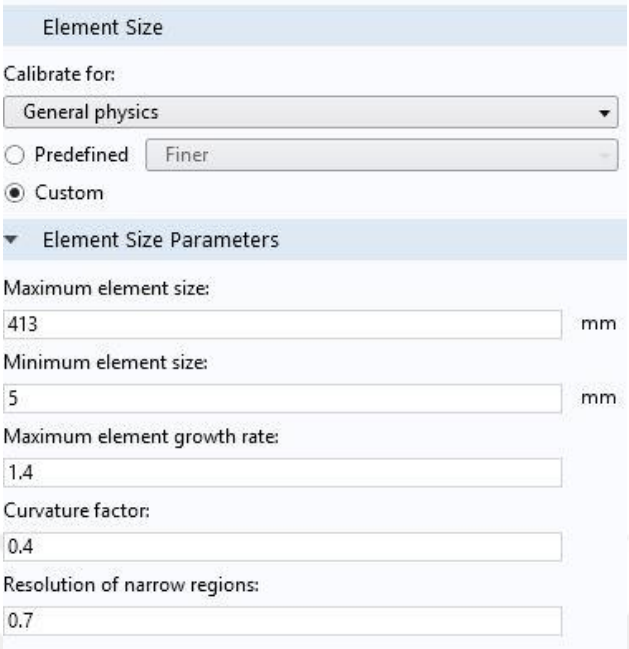


Figure 30 Element size parameters

The lower values of element size parameters except resolution of narrow regions yield a finer mesh in other words more elements. The approximation of a solution can be made better with increased number of elements. However, it requires longer time and more RAM to solve problems with more elements.

4.2.4 Solver

The stationary study in which electrochemical variables do not change over time was used in this thesis work since the effectiveness of cathodic protection system was tested only under steady-state conditions. The algorithm used for solving the non-linear finite element problem was Newton-Raphson method. The multiple iterations were taken until the solution was converged to within the desired tolerance. A convergence plot shows the error of estimate for each iteration number [49]. The error should decrease if the solution is converged. One of the convergence plots of the non-linear solution for cathodic protection modeling was given in Figure 31.

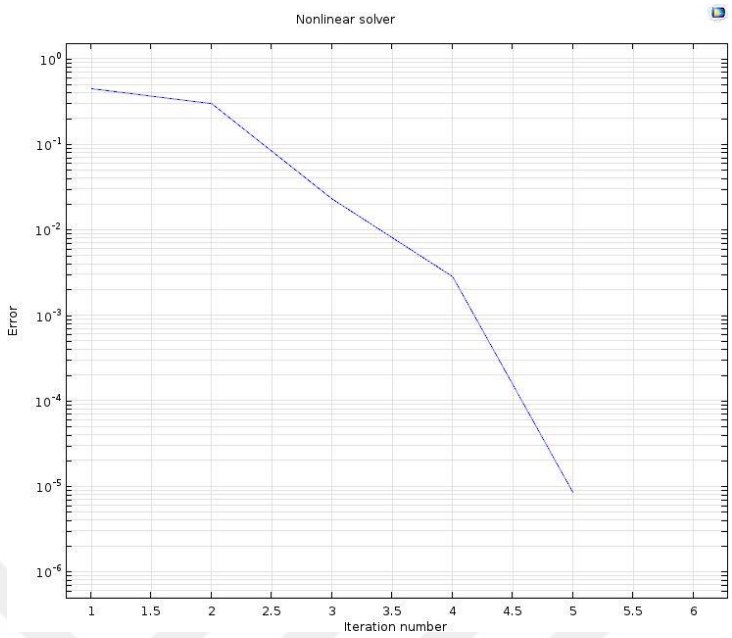


Figure 31 Convergence plot of nonlinear solver

It is desired to take as few Newton-Raphson steps as possible when solving problems with too many degrees of freedom. COMSOL uses a damping factor to improve convergence and minimize the number of steps. A minimum damping factor of 10^{-6} was used for 1109275 degrees of freedoms (DOF) including 374496 internal DOFs in this study.

4.2.5 Cathodic Protection Simulation for the Hull Structures

The cathodic protection application for an amphibious vehicle was constructed with eight sacrificial anodes having 135x70x22 mm dimensions placed on proper locations of the vehicle hull. The anodes and their relative positions are displayed in the model geometry as seen in Figure 32 and Figure 33. The anodes are marked as red shaded rectangles in these figures. The positions of sacrificial anodes were determined after many trials.

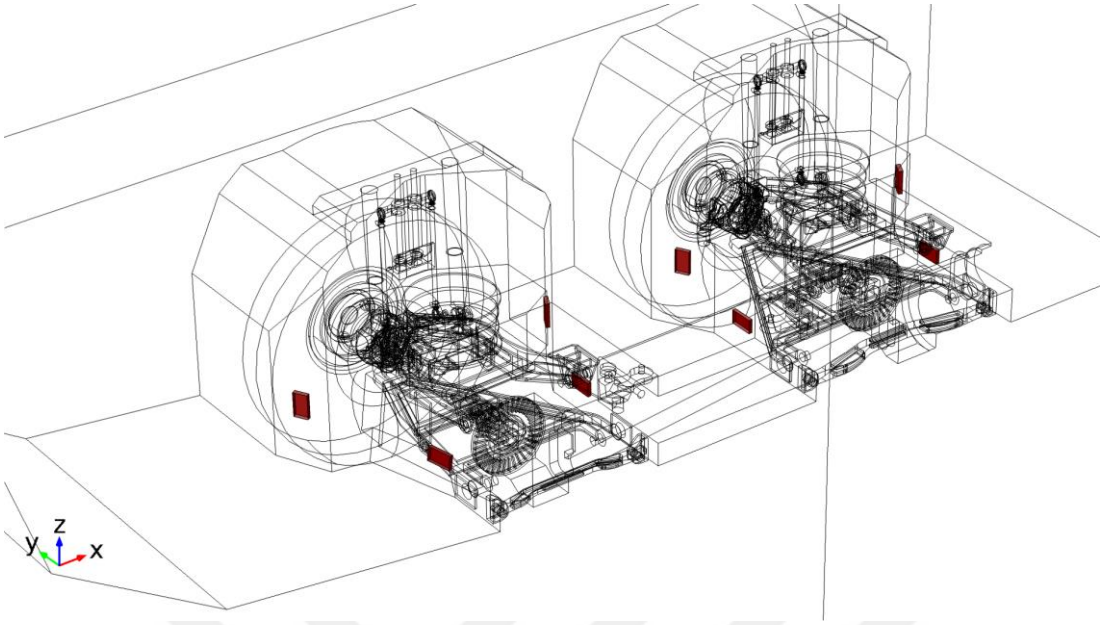


Figure 32 Highlighted anodes in the vehicle hull

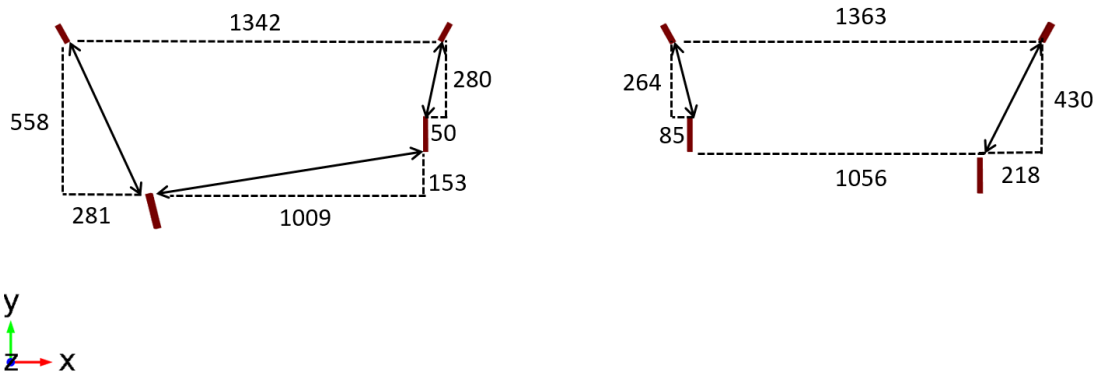


Figure 33 Relative anode positions in millimeters in the vehicle hull on xy plane

The simulation result as shown in Figure 34 revealed that almost uniform potential distribution was maintained on the steel surfaces. It was seen that even the highest surface potential of -844 mV on the brake disk satisfied the selected protection criteria. The potentials on the surfaces near the anodes were relatively lower than other surfaces. The existing cathodic protection design was also simulated for comparison. The results are given in APPENDIX III.

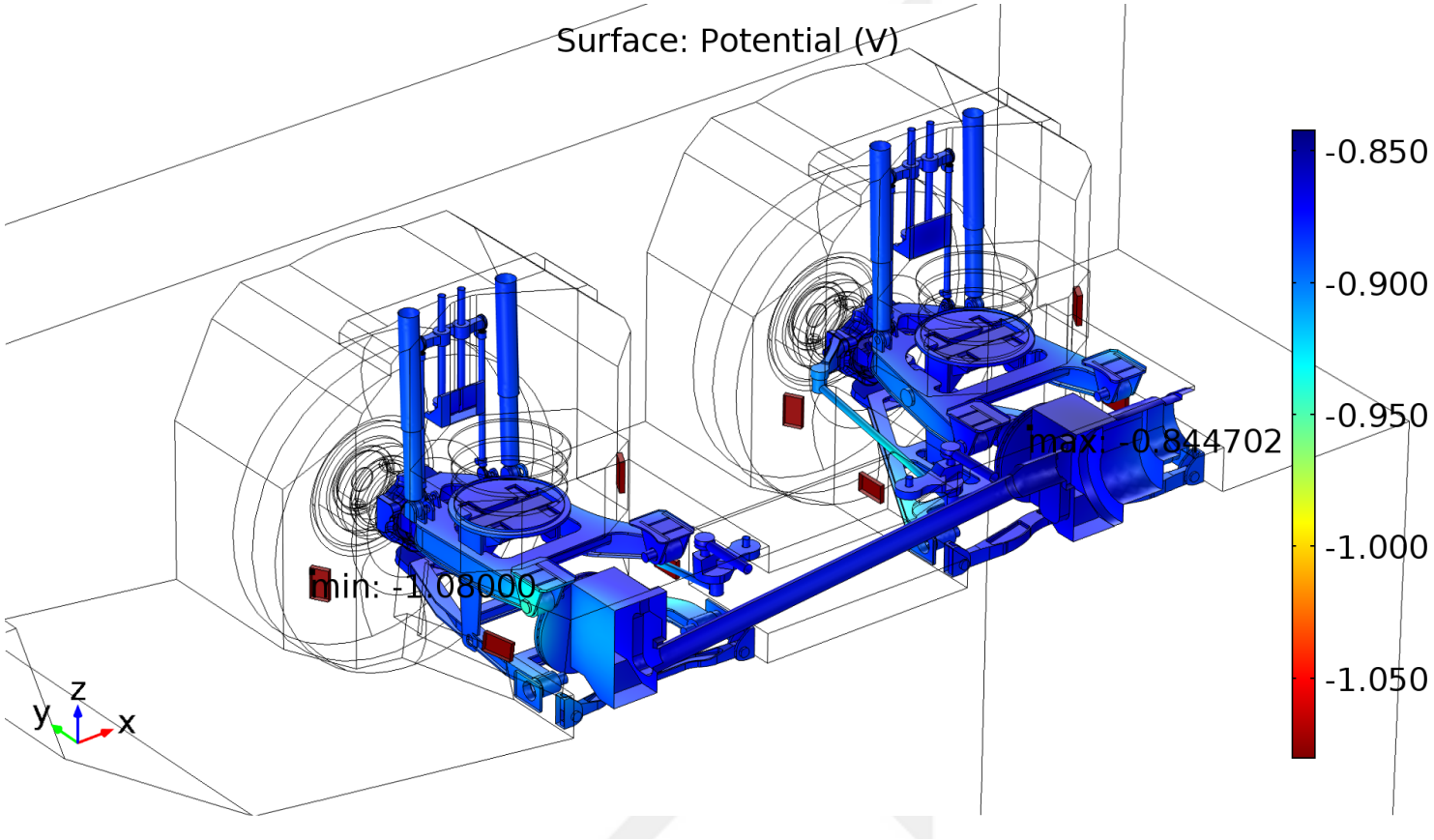


Figure 34 The resulting potential distribution on the steel surfaces with 8 anodes

The most problematic region detected from the vehicles in service was the concave surface at the joint between wheel axle and wheel hub. The surface was shielded by its own geometry. Although, the selected protection potential was maintained on the surface, it was desired to lower the potential even more for better protection. For this reason, two pencil type anodes, having dimensions of 5 mm radius and 25 mm length, were preferentially placed on the upper and the lower wishbones near the component (see Figure 35) while other eight anodes were kept at their previous locations.

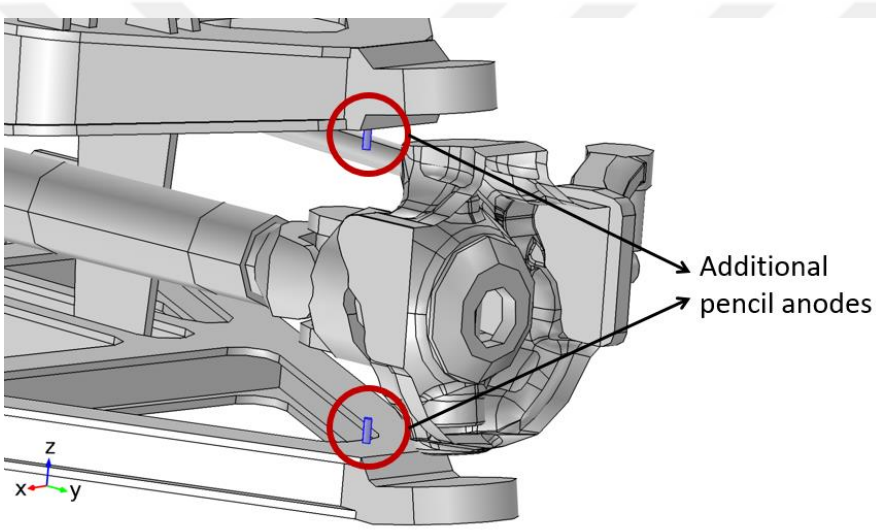


Figure 35 Additional pencil anodes placed near the wheel hub

The optimized simulation for the concave surfaces of the wheel hub was computed with additional pencil anodes. The distribution of surface potential on the bare steel was not effected significantly expect the surfaces close to pencil anodes. The effectiveness of protection by the existing cathodic protection system (given in APPENDIX III) designed system without additional pencil anodes and the modified system in this study for the wheel hubs are compared as seen in Figure 36. It can be conveniently said that the optimization was very effective in lowering the surface potential on the wheel hubs.

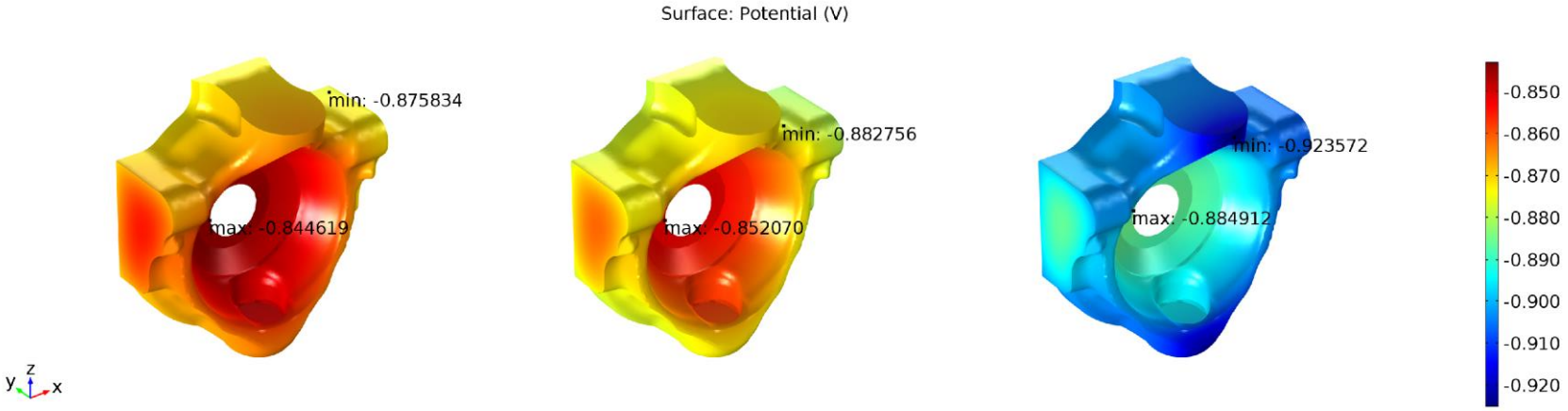


Figure 36 Comparison of the effectiveness of different situations on the wheel hub: existing (left), designed (center) and modified (right) systems

All the steel components were supposed to be coated during the service life of the amphibious vehicles. However, the coating layer may fail on specific regions randomly. The common problematic areas were detected after many observations on the vehicles in service during maintenance. In order to simulate situations when the coating layer failed, boundary conditions were assigned only on the commonly damaged partial surfaces such as axle joints, control arms, supporting rods, wheel hubs and upper and lower wishbones (highlighted in Figure 37). The rest of the steel components were considered isolated and assumed to have no effect on the cathodic protection system.

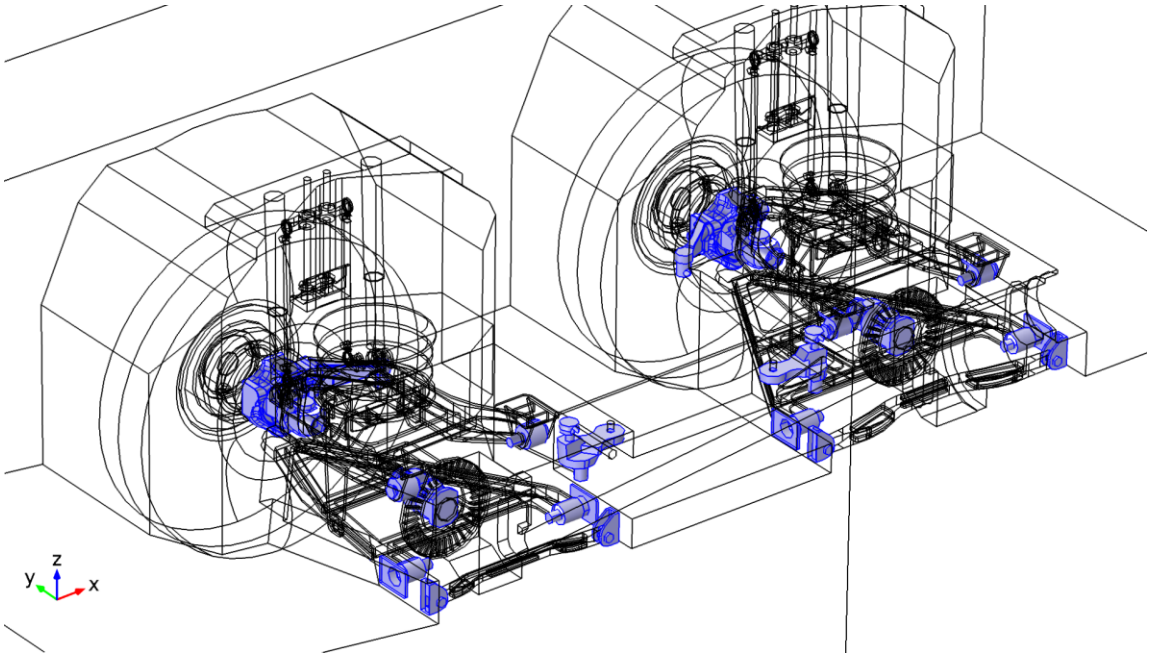


Figure 37 The locations of uncoated areas in the hull structure

The simulation was repeated without changing parameters and anode geometry. It can clearly be seen in Figure 38 that the resulting potentials on the uncoated surfaces were more negative than the previous case as expected. Higher surface over-potentials were determined due to reduction in current demand as the total active steel surface area was reduced.

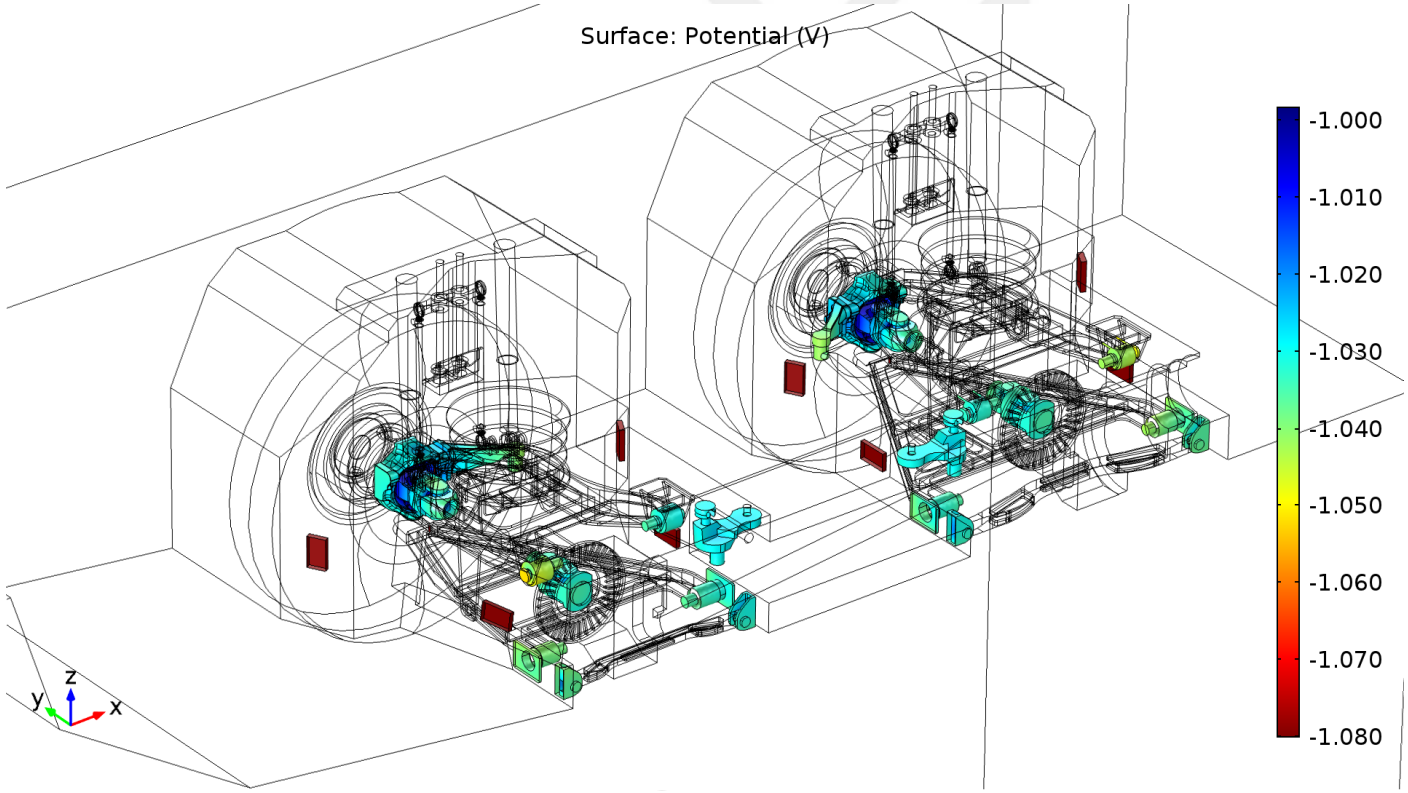


Figure 38 The resulting potential distribution on the uncoated steel surfaces

The mounted anodes were more than adequate for the cathodic protection when the cathode area was reduced to 2.25 m^2 which was approximately 17% of the total surface area of steel components. The higher over-potential values are undesired because excessive cathodic polarization on the steel surfaces increases hydrogen evolution reaction rates. In order to avoid hydrogen embrittlement and hydrogen induced stress corrosion cracking on the bare steel surfaces, the number of anodes should be decreased. The anodes mounted on the vehicle body and one of the pencil anodes on the wishbones near the wheel hubs, were removed. Instead, additional pencil anodes, having 50 mm length and 5 mm radius, were placed near the geometric center of uncoated surfaces to establish a new protection system configuration (see Figure 39).

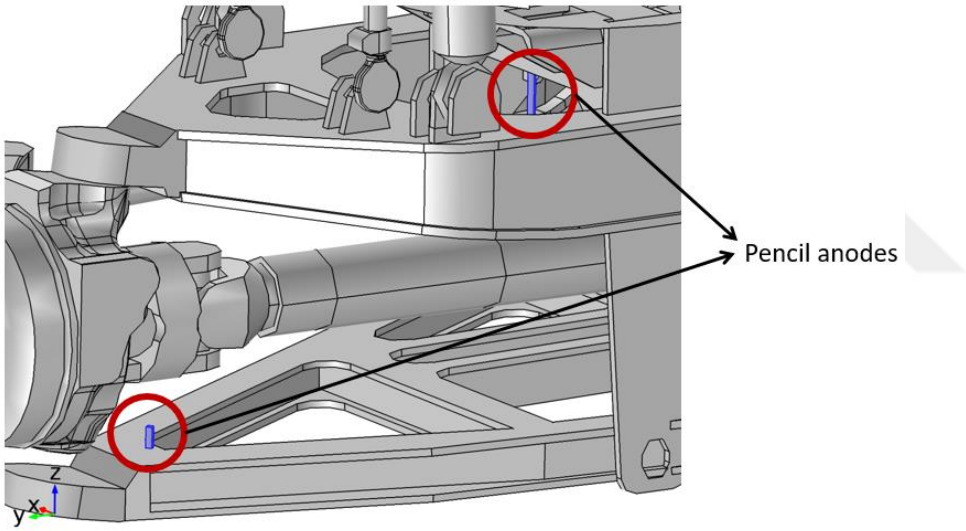


Figure 39 Pencil anodes' loactions for reduced steel area

The potential distribution from -860 mV to -880 mV was maintained on the bare surfaces as seen in Figure 40. The anode requirement to protect only these areas was decreased for the selected protection potential. There may be countless cases where the paint deficient areas vary both in size and locations on the steel surfaces. The anode configuration in the last protection modeling should be utilized as a supplementary application to the existing or designed cathodic protection system for better protection against probable paint defects.

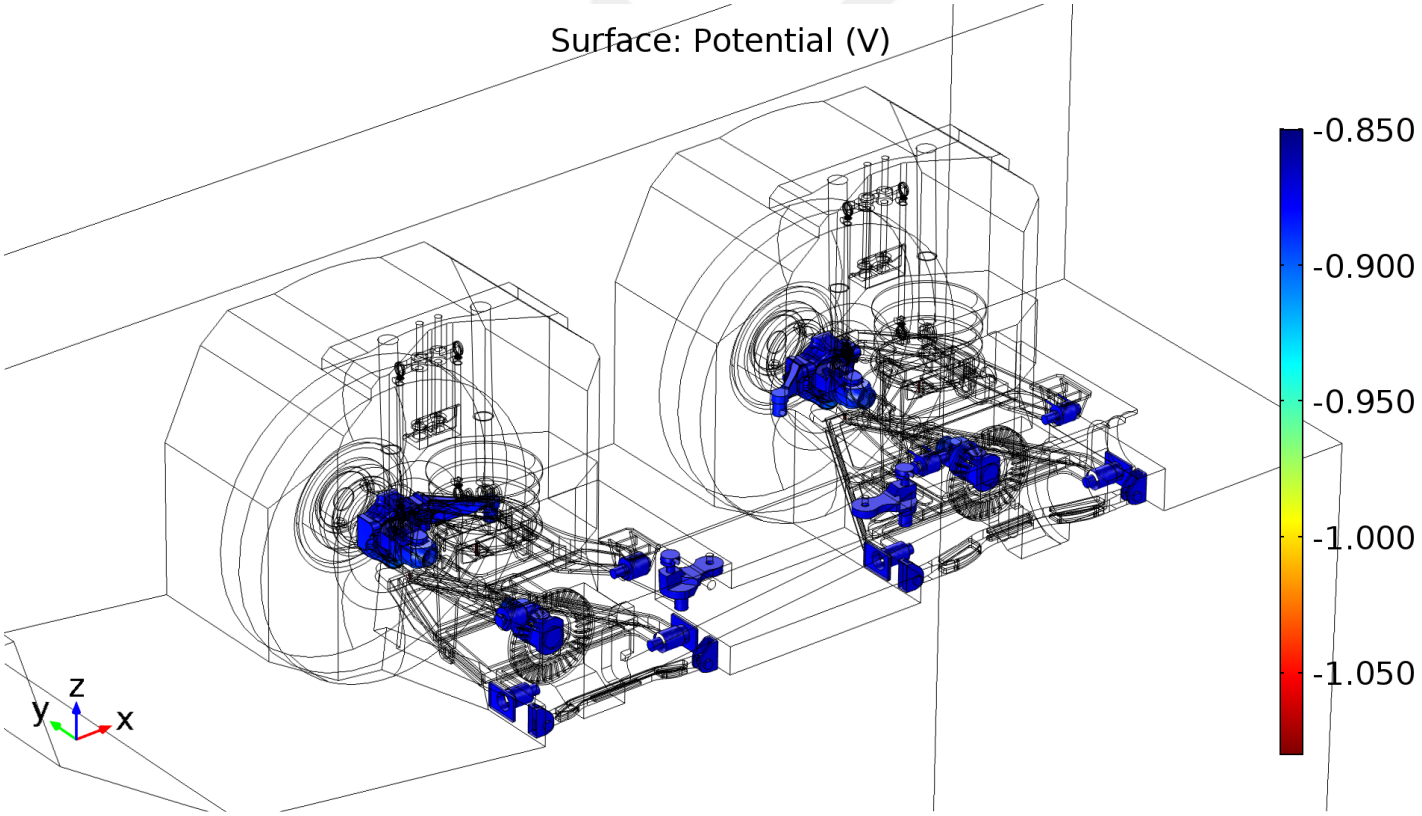


Figure 40 The reduced amount of anodes for paint deficient areas

CHAPTER 5

CONCLUSIONS

Amphibious vehicles are designed to operate both on land and in water. The oxide formation on uncoated steel surface is accelerated in seawater and in marine environment. Electrochemical tests were applied to the selected steel grades of an amphibious vehicle. The polarization curves were interpreted to obtain kinetic information on corrosion behavior for low alloy and carbon steels. The cathodic polarization behavior was affected by the limiting current due to the concentration changes near the interface between the steel surface and the electrolyte. The limiting current density was derived from the cathodic branch of the polarization curves.

The electrochemical data obtained for AISI 4140 steel were used to simulate cathodic protection application via COMSOL Multiphysics. The quantity and current output of anodes were calculated according to the recommended practice by Det Norske Veritas [30]. Then, the anodes were placed to the proper places on the vehicle hull. The current was supplied from the sacrificial anodes to the bare steel surfaces to attain at least the critical protection potential. It was seen that eighth anodes having 135x70x22 mm dimensions mounted on the body of the vehicle were sufficient to polarize steel components to the values below the selected critical protection potential of -843 mV. It should be noted that the steel area under the sacrificial anode must be well-isolated. Otherwise, it may result in very high surface over-potentials on those areas.

The problematic areas detected after many field observations were assigned as the bare steel surfaces for another case of the cathodic protection simulation. When the anode configuration was not modified, relatively more negative potentials were observed on the uncoated surfaces. Lowering the potential on the bare steel surfaces further may revitalize hydrogen evolution as the cathodic reaction. Although, over-protection is unlikely to occur on the steel surfaces with the Al-Zn-In anodes used in

this study, there is always a possibility of hydrogen embrittlement due to the atomic diffusion of hydrogen from the interface between the surface of the steel component and seawater. Moreover, the entire coating layer of a component might be peeled off due to intensive reactions on the bare steel surfaces starting from a minor defect. Thus, anode size and dimensions were further reduced to converge to the protective potential values for the case when bare steel surface was reduced.

In conclusion, cathodic protection with the minimum amount of sacrificial anodes was accomplished for the hull structures in seawater. Potential distribution on the uncoated steel surfaces was quite reasonable for preventing corrosion in the light of the assumptions in the modeling. The output of this study can be taken as a reference for the practical application of cathodic protection for the hull structures of amphibious vehicles.

REFERENCES

[1] Joint Staff J-7, *DOD Dictionary of Military and Associated Terms*. Joint Electronic Library, 2016.

[2] US Navy and The Joint Staff, *JP 3-02: Amphibious Operations*. Joint Electronic Library, 2014.

[3] Department of the Army, *Combined Arms Gap-Crossing Operations*. Army Knowledge Online, 2008.

[4] army-technology.com, "M3 Amphibious Bridging and Ferrying System, Germany." [Online]. Available: http://www.army-technology.com/projects/m3amphibiousbridging/m3amphibiousbridging1.html. [Accessed: 01-Dec-2016].

[5] National Materials Advisory Board, *Materials for Lightweight Military Combat Vehicles*. National Academy Press, 1982.

[6] A. Kumar, L. D. Stephenson, and R. H. Heidersbach, "Corrosion Control for Military Facilities," in *ASM Handbook Corrosion: Environments and Industries*, vol. 13C, ASM International, 2006, pp. 141–147.

[7] Under Secretary of Defense (Acquisition Technology and Logistics), *Efforts to Reduce Corrosion on the Military Equipment and Infrastructure of the Department of Defense*. Office of the Secretary of Defense, USA, 2007.

[8] The Open University, *Seawater: Its Composition, Properties and Behaviour*, 2nd ed. Elsevier, 1995.

[9] M. G. Fontana, *Corrosion Engineering*, 3rd ed. McGraw-Hill Book Company, 1987.

[10] W. R. Revie and H. H. Uhlig, *Corrosion and Corrosion Control*, 4th ed. John Wiley & Sons, 2008.

[11] E. Protopopoff and P. Marcus, "Potential Measurements with Reference Electrodes," in *ASM Handbook Corrosion: Fundamentals, Testing, and*

Protection, vol. 13A, ASM International, 2003, pp. 13–16.

[12] D. W. Shoesmith, "Kinetics of Aqueous Corrosion," in *ASM Handbook Corrosion: Fundamentals, Testing, and Protection*, vol. 13A, 2003, pp. 42–51.

[13] J. Newman and K. E. Thomas-Alyea, *Electrochemical Systems,3rd edition*, 3rd ed. John Wiley & Sons, 2004.

[14] M. Stern and A. L. Geary, "Electrochemical Polarization I. A Theoretical Analysis of the Shape of Polarization Curves," *J. Electrochem. Soc.*, vol. 104, no. 1, pp. 56–63, 1957.

[15] J. Tafel, "Über die Polarisation bei kathodischer Wasserstoffentwicklung," *Zeit. Phys. Chem.*, vol. 50A, no. 641, 1905.

[16] G. T. Burstein, "A hundred years of Tafel's Equation: 1905-2005," *Corros. Sci.*, vol. 47, no. 12, pp. 2858–2870, 2005.

[17] V. C. Wagner and W. Traud, "On the Interpretation of Corrosion Processes Through the Superposition of Electrochemical Partial Processes and on the Potential of Mixed Electrodes," *Elektrochemie und Angew. Phys. Chemie*, vol. 44, no. 7, pp. 391–402, 1938.

[18] F. Mansfeld, "Classic paper in corrosion science and engineering with a perspective by F. Mansfeld," *Corrosion*, vol. 62, no. 10, pp. 843–844, 2006.

[19] N. Perez, *Electrochemistry and Corrosion Science*. Kluwer Academic Publishers, 2004.

[20] G. S. Frankel, "Fundamentals of Corrosion Kinetics," in *Active Protective Coatings*, A. E. Hughes, J. M. C. Mol, M. L. Zheludkevich, and R. G. Buchheit, Eds. Springer Netherlands, 2016, pp. 17–32.

[21] I. Matsushima, "Carbon Steel-Corrosion by Seawater," in *Uhlig's Corrosion Handbook*, 3rd ed., R. W. Revie, Ed. John Wiley & Sons, Inc., 2011, pp. 601–607.

[22] M. Pourbaix, *Atlas of Electrochemical Equilibria in Aqueous Solutions*.

National Association of Corrosion Engineers, 1974.

[23] P. R. Roberge, *Corrosion Engineering, Principles and Practice*. Mg-Graw Hill, 2008.

[24] S. A. Bradford, *Corrosion Control*, 2nd ed. CASTI Publishing Inc., 2001.

[25] A. D. Jones, *Principles and Prevention of Corrosion*, 2nd ed. Prentice-Hall Inc, 1996.

[26] F. Mansfeld, "Electrochemical Methods of Corrosion Testing," in *ASM Handbook Corrosion: Fundamentals, Testing, and Protection*, vol. 13A, ASM International, 2003, pp. 446–462.

[27] Einar Bardal, *Corrosion and Protection*. Springer, 2004.

[28] NACE Standard, "NACE RP0176 - Control of Corrosion on Steel, Fixed Offshore Platforms Associated with Petroleum Production," 1976.

[29] J. H. Fitzgerald III, "Engineering of Cathodic Protection Systems," in *Uhlig's Corrosion Handbook*, 3rd ed., R. W. Revie, Ed. John Wiley & Sons, 2011, pp. 1001–1011.

[30] Det Norske Veritas, "Recommended Practice Cathodic Protection Design," 2010.

[31] NACE Standard, "RP0193 - External Cathodic Protection of On-Grade Carbon Steel Storage Tank Bottoms," 2001.

[32] United States Naval Academy, "Catodic Protection Design." [Online]. Available: https://www.usna.edu/NAOE/_files/documents/Courses/EN380/Cathodic Protection Design.pdf. [Accessed: 18-Jan-2017].

[33] V. Ashworth, "Principles of Cathodic Protection," in *Shreir's Corrosion*, 1st ed., Elsevier, 2009, pp. 2747–2762.

[34] ASTM International, “Standard Guide for Development and Use of a Galvanic Series for Predicting Galvanic Corrosion Performance, G82-98,” 2014.

[35] Headquartes Department of the Army, “Technical Manual: Electrical Design, Cathodic Protection,” 1985.

[36] R. H. Heidersbach, “Cathodic Protection,” in *ASM Handbook Corrosion: Fundamentals, Testing, and Protection*, vol. 13A, ASM International, 2003, pp. 855–870.

[37] C. F. Schrieber, “Relationship of Chemical Components and Impurities of Aluminum Galvanic Anodes Upon the Cathodic Protection of Marine Structures,” in *Designing Cathodic Protection Systems for Marine Structures and Vehicles, ASTM STP 1370*, H. P. Hack, Ed. American Society for Testing and Materials, 1999.

[38] S. L. D. Carvalho, J. C. F. Telles, and L. R. M. de Miranda, “On the Effect of Some Critical Parameters in Cathodic Protection Systems: A Numerical/Experimental Study,” in *Computer Modeling in Corrosion*, R. S. Munn, Ed. ASTM, 1992, pp. 277–291.

[39] O. W. Siebert, “Laboratory Electrochemical Test Methods,” in *Laboratory Corrosion Tests and Standards, ASTM STP 866*, G. S. Haynes and R. Baboian, Eds. American Society for Testing and Materials, 1985, pp. 65–90.

[40] ASTM International, *Standard Practice for the Preparation of Substitute Ocean Water, D1141-98*. 2013.

[41] K. Maksymiuk, A. Michalska, A. Kisiel, and Z. Galus, “Mercury Electrodes,” in *Handbook of Reference Electrodes*, G. Inzelt, A. Lewenstam, and F. Scholz, Eds. Springer-Verlag Berlin Heidelberg, 2013, pp. 105–106.

[42] H. Kahlert, “Reference Electrodes,” in *Electroanalytical Methods: Guide to Experiments and Applications*, Second Edi., F. Scholz, Ed. Springer-Verlag Berlin Heidelberg, 2010, pp. 291–308.

[43] “Gamry eChem Analyst version 6.25.” Gamry Instruments, Inc.

[44] C. Ponce-De-León, C. T. J. Low, G. Kear, and F. C. Walsh, “Strategies for the

determination of the convective-diffusion limiting current from steady state linear sweep voltammetry," *J. Appl. Electrochem.*, vol. 37, no. 11, pp. 1261–1270, 2007.

[45] ASTM International, *Standard Practice for Calculation of Corrosion Rates and Related Information from Electrochemical Measurements, G102-89*. 1999.

[46] COMSOL MultiPhysics 5.2, *Electrode Kinetics Expressions, Help Notes*. COMSOL Inc.

[47] W. Frei, "Meshing Considerations for Linear Static Problems," 2013. [Online]. Available: https://www.comsol.com/blogs/meshing-considerations-linear-static-problems/. [Accessed: 11-Feb-2017].

[48] A. Griesmer, "Size Parameters for Free Tetrahedral Meshing in COMSOL Multiphysics," *2014*. [Online]. Available: https://www.comsol.com/blogs/size-parameters-free-tetrahedral-meshing-comsol-multiphysics/. [Accessed: 11-Feb-2017].

[49] W. Frei, "Solving Nonlinear Static Finite Element Problems," 2013. [Online]. Available: https://www.comsol.com/blogs/solving-nonlinear-static-finite-element-problems/. [Accessed: 11-Feb-2017].

APPENDIX I

Tables:

Table A-1 Stock solutions used in artificial seawater preparation

Stock Soln.	Compound	Concentration g/L
No. 1	$MgCl_2.6H_2O$	555.6
	$CaCl_2$	57.9
	$SrCl_2.6H_2O$	2.1
No. 2	KCl	69.5
	$NaHCO_3$	20.1
	KBr	10.0
	H_3BO_3	2.7
	NaF	0.3

Table A-2 Chemical compositions by weigth percent of alloying elements in commercial Al-Zn-In galvanic anodes

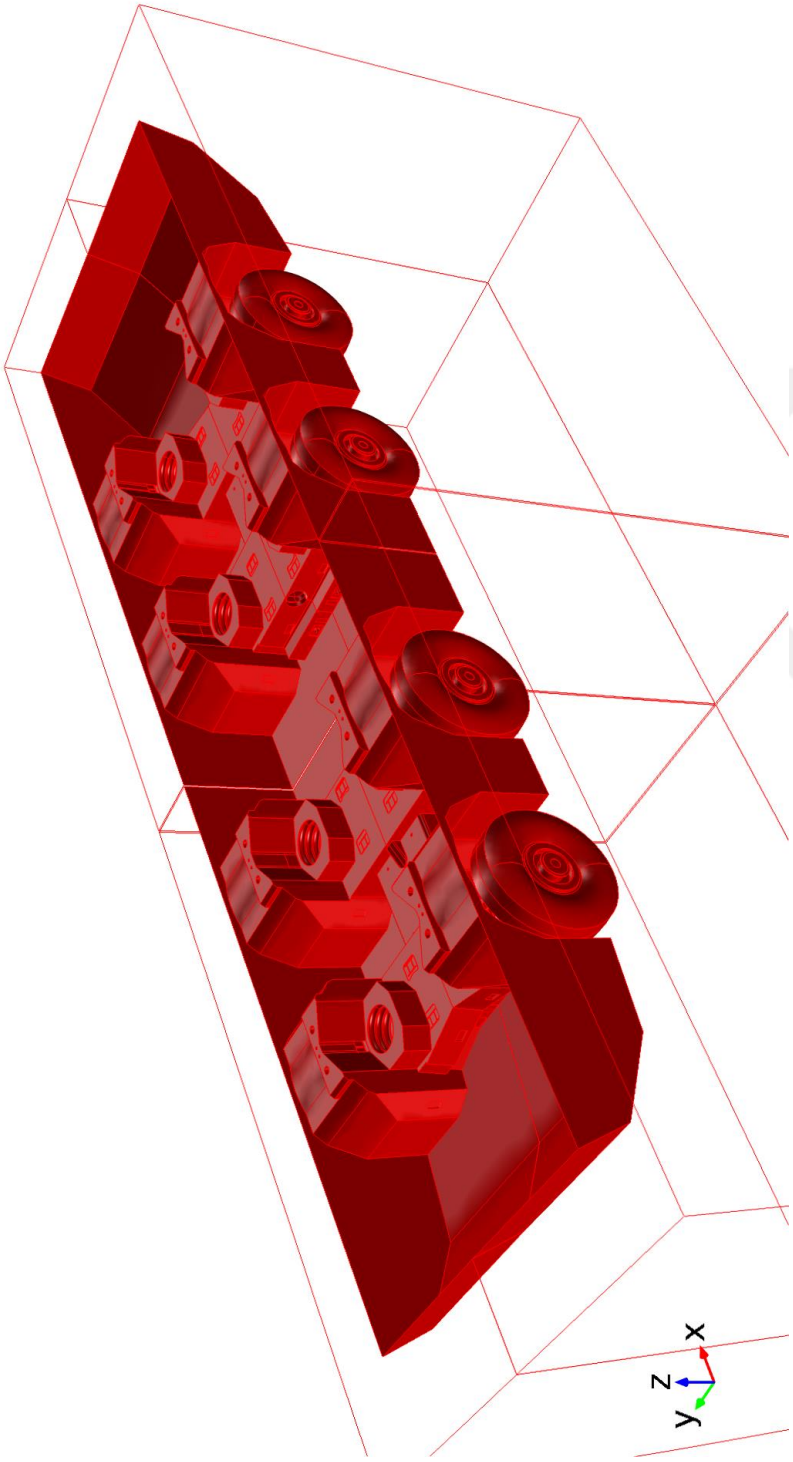
Elements	Coral® "A" Grade	Galvanum® III
Zn	3.5-5.0	2.0-6.0
In	0.015-0.025	0.01-0.02
Cu	max. 0.003	max. 0.006
Fe	max. 0.09	max. 0.13
Si	max. 0.10	0.08-0.20
Others (each)	max. 0.020	max. 0.02
Al	balance	balance

Table A-3 Performance data of the commercial galvanic anodes in seawater

Property	Coral® "A" Grade	Galvanum® III
Capacity, A·h/kg	2585	2535-2650
Closed circuit potential, V wrt Ag/AgCl (seawater)	-1.09	-1.10

APPENDIX II

Full geometry of the amphibious vehicle consisting of the hull structures



APPENDIX III

The existing cathodic protection design with 8 anodes

